

DEVELOPMENTAL BIOLOGY

G protein–coupled receptors control the sensitivity of cells to the morphogen Sonic Hedgehog

Ganesh V. Pusapati,^{1*} Jennifer H. Kong,^{1*} Bhaven B. Patel,¹ Mina Gouti,^{2†} Andreas Sagner,² Ria Sircar,¹ Giovanni Luchetti,¹ Philip W. Ingham,^{3,4} James Briscoe,² Rajat Rohatgi^{1‡}Copyright © 2018
The Authors, some
rights reserved;
exclusive licensee
American Association
for the Advancement
of Science. No claim
to original U.S.
Government Works

The morphogen Sonic Hedgehog (SHH) patterns tissues during development by directing cell fates in a concentration-dependent manner. The SHH signal is transmitted across the membrane of target cells by the heptahelical transmembrane protein Smoothed (SMO), which activates the GLI family of transcription factors through a mechanism that is undefined in vertebrates. Using CRISPR-edited null alleles and small-molecule inhibitors, we systematically analyzed the epistatic interactions between SMO and three proteins implicated in SMO signaling: the heterotrimeric G protein subunit $G\alpha_s$, the G protein–coupled receptor kinase 2 (GRK2), and the $G\alpha_s$ -coupled receptor GPR161. Our experiments uncovered a signaling mechanism that modifies the sensitivity of target cells to SHH and consequently changes the shape of the SHH dose-response curve. In both fibroblasts and spinal neural progenitors, the loss of GPR161, previously implicated as an inhibitor of basal SHH signaling, increased the sensitivity of target cells across the entire spectrum of SHH concentrations. Even in cells lacking GPR161, GRK2 was required for SHH signaling, and $G\alpha_s$, which promotes the activation of protein Kinase A (PKA), antagonized SHH signaling. We propose that the sensitivity of target cells to Hedgehog morphogens, and the consequent effects on gene expression and differentiation outcomes, can be controlled by signals from G protein–coupled receptors that converge on $G\alpha_s$ and PKA.

INTRODUCTION

Secreted ligands of the Hedgehog (Hh) family function as morphogens and pattern tissues, such as the spinal cord, limb bud, and paraxial mesoderm, during development. Activation of the Hh signaling pathway in responsive cells can drive the patterning of spinal neural progenitor subtypes in a manner that depends on both the concentration of the ligand Sonic Hedgehog (SHH) and the duration of SHH exposure (1). The mechanism by which extracellular SHH is transformed into the transcriptional activity that controls target cell identity remains an unresolved question, partly because the mechanisms that convey Hh signals from the cell surface to the nucleus are incompletely understood.

Patched (PTCH) proteins, the transmembrane receptors for Hh ligands, repress the activity of Smoothed (SMO), a frizzled family G protein (heterotrimeric guanine nucleotide–binding protein)–coupled receptor (GPCR) that transmits the Hh signal across the membrane to the cytoplasm. In the absence of Hh ligands, protein kinase A (PKA) and Suppressor of Fused (SUFU) inhibit the activity of the glioma-associated oncogene family transcription factors GLI2 and GLI3 and promote the proteolysis of GLI3 into a transcriptional repressor fragment (hereafter called GLI3R) (2). Hh ligands inactivate PTCH1, allowing SMO to adopt an active conformation and accumulate in the membrane of the primary cilium (3). Active SMO ultimately antagonizes the inhibitory effect of PKA and SUFU on the GLI proteins. As a result, the formation of GLI3R is blocked, and full-length GLI2

and GLI3 are converted to transcriptional activators (hereafter GLI2A and GLI3A) (4–7).

The mechanism by which the Hh signal is transmitted from SMO to GLI2 or GLI3 remains poorly understood in vertebrates. Given the negative role of PKA in Hh signaling in all animals, SMO must somehow antagonize PKA activity or shield GLI proteins from the inhibitory influence of PKA. Several proteins that can influence PKA activity have been found to play a role in signaling at the step between SMO and GLI2 or GLI3. Recent work focused on a key role for the ciliary GPCR GPR161, which has been proposed to function downstream of SMO to repress basal signaling (signaling in the absence of Hh ligands) by promoting the production of GLI3R (8). GPR161 activates the $G\alpha_s$ heterotrimeric G protein, encoded by the *Gnas* gene, leading to increases in cyclic adenosine 3',5'-monophosphate (cAMP) levels and, consequently, elevated PKA activity. GPR161 is localized in the ciliary membrane but is cleared from cilia when Hh ligands are received, a step which requires the activity of GPCR kinase 2 (GRK2) (9, 10). Consistent with this model, GRK2 activity has been shown to be required for propagation of the Hh signal in multiple systems (9, 11–17), and $G\alpha_s$, like GPR161, functions as a negative regulator of the Hh pathway (18–21). In summary, a widely invoked model for cytoplasmic Hh signaling in vertebrates posits that Hh ligands antagonize GLI3R production by clearing GPR161 from cilia, a step mediated by GRK2, and, consequently, $G\alpha_s$ activity (8, 9).

However, this model is not fully consistent with neural tube patterning phenotypes in mouse embryos carrying mutations in genes encoding many of these components (8, 13, 18, 22). For example, neural tube patterning in *Gpr161*^{−/−} embryos is more severely disrupted than that in *Gli3*^{−/−} embryos, suggesting that the resulting phenotype is due to more than a loss of GLI3R (8, 23). Conversely, defects in *Gpr161*^{−/−} embryos are less severe than those in *Gnas*^{−/−}, *Ptch1*^{−/−}, and *Sufu*^{−/−} embryos or in embryos lacking PKA activity (8, 18, 22). The epistatic relationship between SMO and GPR161 is also ambiguous. GPR161 is epistatic to SMO when assaying Hh-induced differentiation

¹Departments of Medicine and Biochemistry, Stanford University School of Medicine, Stanford, CA 94305, USA. ²The Francis Crick Institute, Midland Road, London NW1 1AT, UK. ³Lee Kong Chian School of Medicine, Nanyang Technological University, Singapore 639798, Singapore. ⁴Living Systems Institute, University of Exeter, Exeter EX4 4RJ, UK.

*These authors contributed equally to this work.

†Present address: Max-Delbrück-Center for Molecular Medicine, Robert-Rössle-Strasse 10, 13125 Berlin, Germany.

‡Corresponding author. Email: rrohathgi@stanford.edu

into NKX6.1-positive neural progenitors, but SMO is epistatic to GPR161 when assaying FOXA2-positive progenitors (8). More generally, the epistatic relationships among SMO, GPR161, $G\alpha_s$, and GRK2 have not been determined.

We set out to test the current model for Hh signaling by SMO using epistasis analysis, quantitative signaling, and differentiation assays in two Hh-responsive cultured cell systems—cultured fibroblasts and spinal neural progenitor cells (NPCs). NPCs differentiate into specific classes of progenitor subtypes in the neural tube in response to different levels of Hh signaling (24, 25), allowing an assessment of the morphogenetic function of this pathway. Our results reveal that GPR161 regulates Hh signaling in two fundamentally different ways. In addition to its established role in repressing basal, or ligand-independent, Hh signaling, GPR161 plays an equally important role in regulating ligand-driven signaling. We found that GPR161 reduced the sensitivity of target cells to SHH, markedly altering the shape of the SHH dose-response curve. Thus, GPR161 influences neural tube patterning by altering target-cell sensitivity to the SHH morphogen. Unexpectedly, GRK2 retained the ability to promote and $G\alpha_s$ retained the ability to restrain Hh signaling in cells lacking GPR161. We propose that target-cell responses to Hh signaling are influenced through both GPR161-dependent and GPR161-independent pathways that are regulated by GRK2 and that converge on $G\alpha_s$ and, ultimately, PKA activity.

RESULTS

GPR161 functions as an attenuator of Hh signaling in NIH/3T3 cells

We used clustered regularly interspaced short palindromic repeats (CRISPR)-mediated editing to generate loss-of-function mutations in the *Gpr161* gene using four different guide RNAs in NIH/3T3 cells, a mouse embryonic fibroblast (MEF) cell line widely used for the mechanistic analysis of Hh signaling in vitro. In contrast to previous observations in *Gpr161*^{-/-} mouse embryos, GLI3R abundance was unaltered in all four *Gpr161*^{-/-} cell lines whether or not the cells were stimulated with SHH (Fig. 1A). The abundance of *Gli1*, a direct Hh target gene used as a measure of signaling strength, was also very similar between wild-type and *Gpr161*^{-/-} cells, both in the absence of SHH or in the presence of a saturating concentration of SHH (Fig. 1A).

Because there was no discernable effect on basal signaling in *Gpr161*^{-/-} cells, we next asked whether signaling responses were altered in response to SHH. The curve depicting the relationship between *Gli1* mRNA and the concentration of SHH was shifted to the left in *Gpr161*^{-/-} cells compared to wild-type cells, resulting in ~3-fold to 5-fold increase in the potency of the ligand (Fig. 1B). The concentration of SHH that resulted in half-maximal increase in *Gli1* mRNA, a formal measure of potency hereafter denoted as EC₅₀, decreased from 1.9 nM in wild-type cells to 0.4 to 0.7 nM in *Gpr161*^{-/-} cells (Fig. 1B). In addition, there was a variable increase in the maximum levels of *Gli1* mRNA induced by SHH in *Gpr161*^{-/-} cells (Fig. 1B). The increase in sensitivity to SHH in *Gpr161*^{-/-} cells is consistent with the neural tube phenotype in *Gpr161*^{-/-} embryos—the dorsal expansion of ventral progenitor domains (8). Wild-type and *Gpr161*^{-/-} cells contained approximately equivalent amounts of GLI3R protein, both at baseline and after exposure to varying doses of SHH (Fig. 1C). Full-length GLI3 levels were modestly increased in cells lacking GPR161 (Fig. 1, A and C), suggesting a defect in the activation of full-length

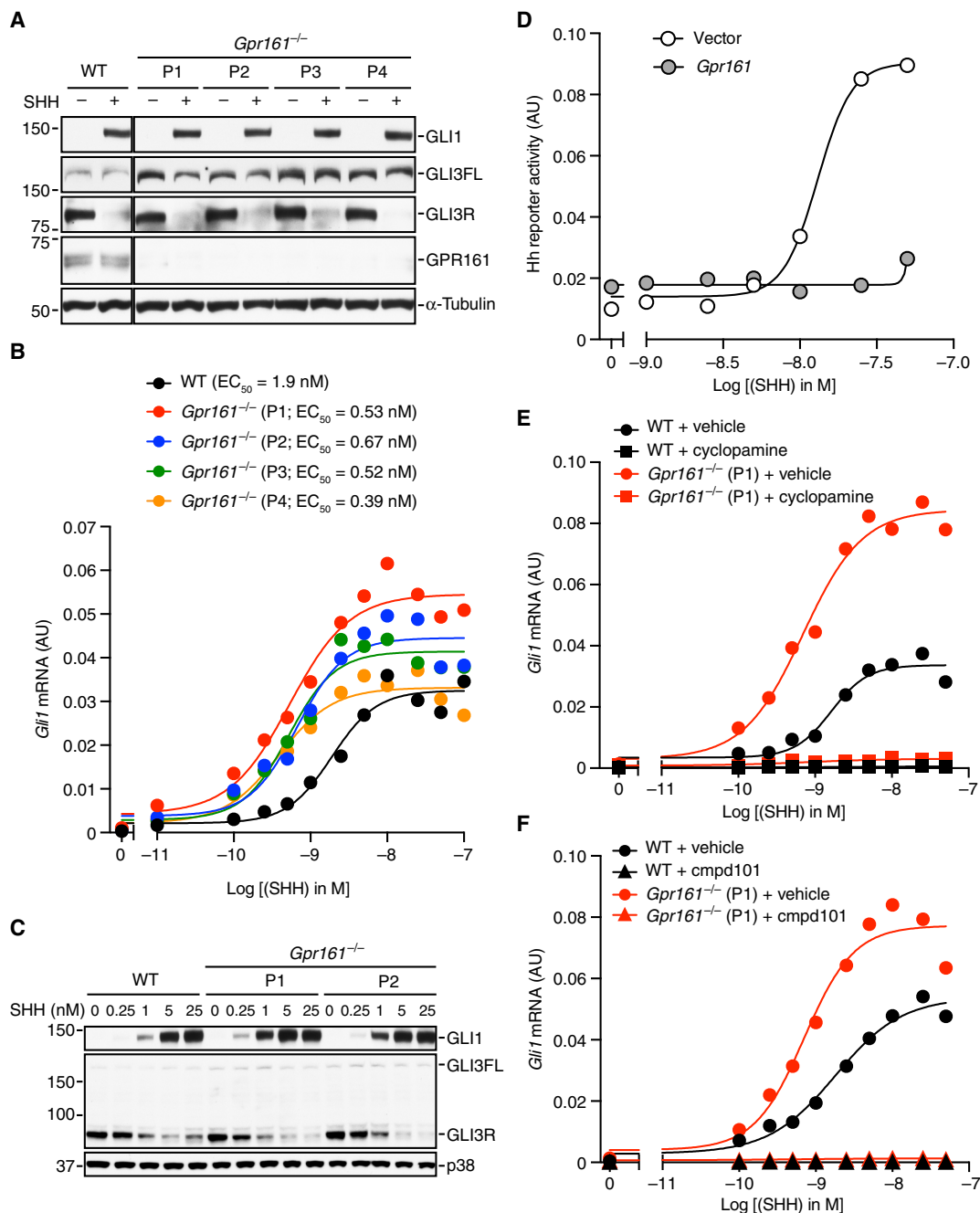
GLI proteins, which are known to be much more unstable in their transcriptionally active states (5). Overexpression of *Gpr161* in NIH/3T3 cells blocked expression of a Hh signaling reporter (Fig. 1D), a phenotype opposite to the enhanced signaling phenotype seen when GPR161 is lost (Fig. 1B).

The increase in sensitivity to SHH in *Gpr161*^{-/-} cells in the absence of changes in the abundance of GLI3R (Fig. 1, A and C) or basal signaling suggested that GPR161 may regulate Hh signaling through additional mechanisms that cannot be accommodated by current models. This notion was further reinforced by the epistatic relationship between SMO, GPR161, and GRK2 in NIH/3T3 cells. SMO activity has been shown to be dispensable for some of the increased Hh responses seen in the neural tubes of mouse embryos lacking GPR161, an observation used to place GPR161 downstream of SMO in the pathway (8). However, SHH-stimulated signaling remained dependent on SMO activity in *Gpr161*^{-/-} NIH/3T3 cells because it could be completely blocked by the SMO antagonist cyclopamine (Fig. 1E). Our epistasis analysis suggests that GPR161 functions in NIH/3T3 cells as a modifier rather than an obligate downstream component of SMO signaling.

Two (nonmutually exclusive) mechanisms have been proposed to explain the positive role of GRK2 in Hh signaling: (i) GRK2 promotes the ciliary localization of SMO, and (ii) GRK2 induces the clearance of GPR161 from the ciliary membrane, leading to a decrease in $G\alpha_s$ and PKA activity (9). The former model has been questioned by recent studies in zebrafish embryos and fibroblasts, showing that SMO accumulates in cilia normally in cells lacking GRK2 activity (9, 17). The latter model is inconsistent with our observation that GPR161 is dispensable for Hh signaling in NIH/3T3 cells (Fig. 1A), whereas GRK2 is essential (17). To establish the epistatic relationship between GRK2 and GPR161, we sought a pharmacological strategy to acutely block the kinase activity of GRK2 and the closely related GRK3. Takeda compound 101 (cmpd101) (26) is a cell-permeable small-molecule inhibitor of both GRK2 and GRK3 (GRK2/3) that can inhibit the desensitization of GPCRs (27). Cmpd101 blocked SHH-driven signaling in NIH/3T3 cells with a median inhibitory concentration (IC₅₀) of 4.9 μ M (fig. S1A), in agreement with the previously reported potency of cmpd101 (IC₅₀ of 3 μ M) in inhibiting the desensitization of μ -opioid receptors in intact cell assays (27). Hh signaling strength was evaluated by measuring (i) the mRNA or protein abundance of *Gli1* and *PTCH1* (both of which are encoded by genes that are directly stimulated by SHH signaling) and (ii) the abundance of GLI3R protein (fig. S1B). The effect of cmpd101 recapitulated the effect of a genetic deletion of *Grk2* in multiple independent clonal cell lines (fig. S1, C to E, and table S1). As reported previously for the genetic ablation of *Grk2*, cmpd101 did not prevent the signal-induced accumulation of SMO in primary cilia (fig. S1F) (9, 17).

If the mechanistic role of GRK2 in Hh signaling is to remove GPR161 from the primary cilium, GRK2 should be dispensable in cells lacking GPR161. However, we found that SHH-induced *Gli1* expression was fully inhibited by cmpd101 in *Gpr161*^{-/-} NIH/3T3 cells, demonstrating that GRK2 must promote Hh signaling in these cells through a mechanism that does not depend exclusively on GPR161 (Fig. 1F). To summarize, our results show that both GRK2 and SMO can function independently of GPR161 in NIH/3T3 cells, a conclusion that is different from the view that SMO and GRK2 promote Hh signaling by antagonizing GPR161 (9). We conclude that GPR161 in NIH/3T3 cells functions as an attenuator of signaling. This should be contrasted with a negative regulator of signaling, such as SUFU, the ablation of

Fig. 1. GPR161 suppresses the potency of Hedgehog ligands in NIH/3T3 cells. (A) Immunoblot showing the indicated proteins in extracts from Sonic Hedgehog (SHH)-treated wild-type (WT) NIH/3T3 cells and four clonal *Gpr161*^{-/-} NIH/3T3 cell lines (P1 to P4) generated using four different guide RNAs. GLI3FL, full-length GLI3; GLI3R, GLI3 transcriptional repressor fragment. (B) Quantification of *Gli1* mRNA relative to glyceraldehyde-3-phosphate dehydrogenase (*Gapdh*) by quantitative reverse transcription polymerase chain reaction (qRT-PCR) in WT and four independently generated *Gpr161*^{-/-} NIH/3T3 cell lines after exposure to the indicated range of SHH concentrations. EC₅₀, concentration that produces a half-maximal response. AU, arbitrary units. (C) Immunoblot showing the indicated proteins in extracts from WT and two different *Gpr161*^{-/-} NIH/3T3 cell lines (P1 and P2) that were either untreated or treated with increasing concentrations of SHH. (D) SHH-induced activation of a luciferase-based Hedgehog (Hh) reporter gene in NIH/3T3 cells transiently transfected with an empty vector or a vector carrying a gene encoding GPR161. (E and F) Quantification of *Gli1* mRNA relative to *Gapdh* by qRT-PCR in WT or *Gpr161*^{-/-} NIH/3T3 cells after exposure to the indicated range of SHH concentrations in the presence or absence of small molecules that inhibit Smoothed (SMO) [cyclopamine (E)] or GPCR kinase 2 (GRK2) [Takeda compound 101 (cmpd101) (F)]. In (B) and (D) to (F), each data point represents a mean of three technical replicates. (A), (B), (E), and (F) show representative data from three independent experiments. (C) and (D) show representative data from two independent experiments.



which leads to SHH-independent activation of signaling that does not depend on SMO (28).

We also tested whether the ciliary localization or clearance of GPR161 could be affected by GRK2 in NIH/3T3 cells. As previously reported, yellow fluorescent protein (YFP)-tagged GPR161 (GPR161-YFP) stably expressed in NIH/3T3 cells accumulated in the ciliary membrane, and the addition of SHH led to the clearance of GPR161-YFP from cilia (fig. S2, A and B) (8). This clearance could be blocked by a small-molecule antagonist of SMO (SANT-1) and by either the genetic ablation of *Grk2* or the inhibition of GRK2 kinase activity by cmpd101 (fig. S2, A and B). Endogenous GPR161 was present at levels too low to detect in NIH/3T3 cilia; however, either the genetic or phar-

macological antagonism of GRK2 led to a marked increase in endogenous GPR161 in cilia, confirming that GRK2 can reduce the abundance of GPR161 in the cilia of NIH/3T3 cells (fig. S2, C and D).

The central piece of evidence that GPR161 is regulated by SMO is the correlative observation that SHH or agonists of SMO can drive the clearance of GPR161 from the ciliary membrane. However, whether the localization of GPR161 in the ciliary membrane (or its clearance) plays a functional role in Hh signaling remains unknown. A C-terminal truncation mutant of GPR161 that cannot be cleared from cilia in response to SHH has no apparent effect on the strength of Hh signaling in cultured cells (9). We also found that the overexpression of *Grk2* could drive GPR161 out of cilia, without leading to activation

of Hh target genes (fig. S2, E to G). Thus, the ciliary clearance of GPR161 can be uncoupled from the activation of Hh signal transduction.

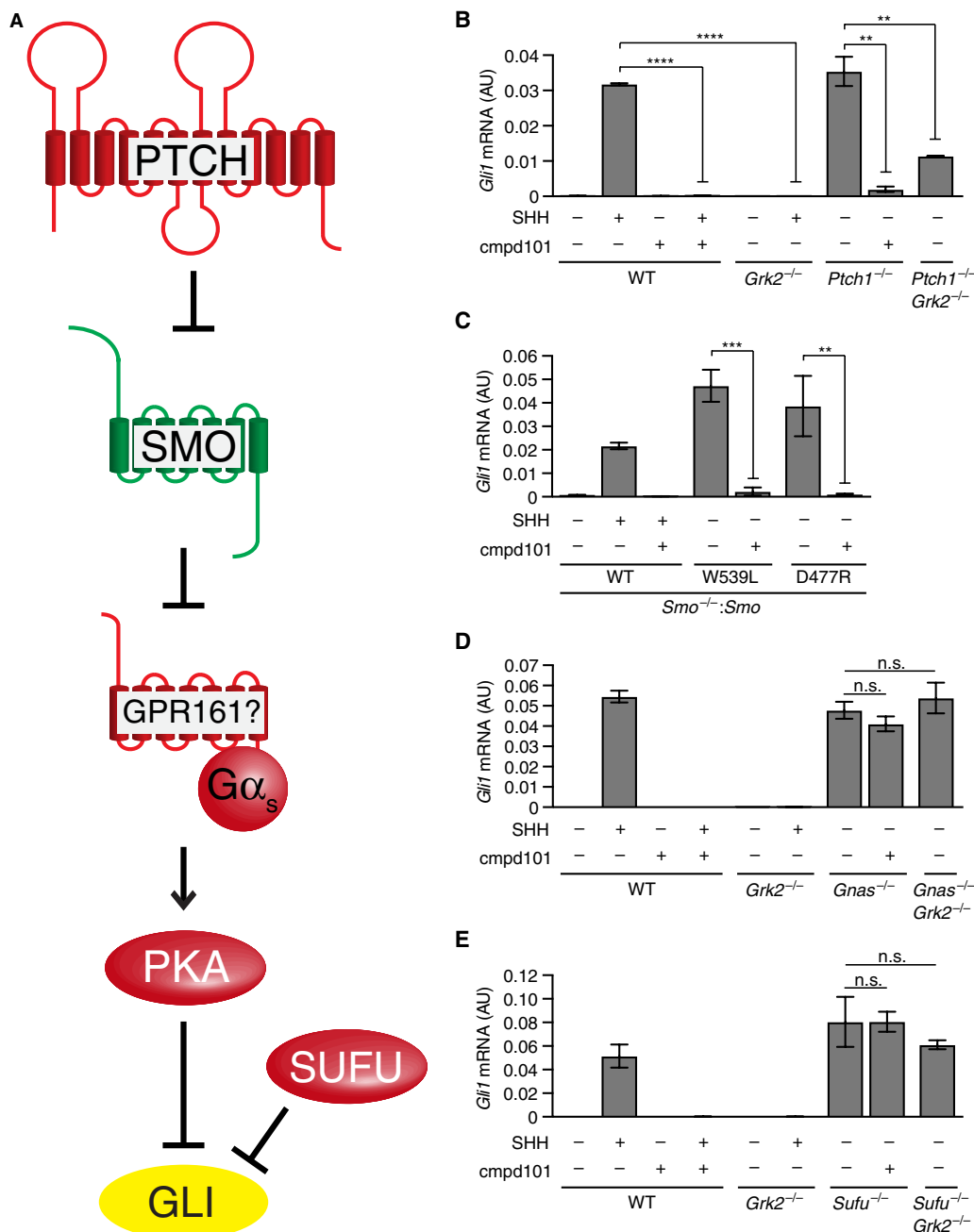
GRK2 functions at a step between SMO and Gα_s in Hh signaling

If GRK2 does not influence Hh signaling by controlling SMO localization (9, 17) or by reducing GPR161 in the primary cilium (Fig. 1F), how does it regulate the pathway? To address this question, we performed a comprehensive epistasis analysis to identify the critical step regulated by GRK2 (Fig. 2A). We generated clonal NIH/3T3 cell lines carrying loss-of-function mutations in genes encoding three negative regulators of the pathway (PTCH1, Gα_s, or SUFU), along with

a cell line expressing a constitutively active, oncogenic mutant form of SMO (SMO-W539L, in which Trp⁵³⁹ is mutated to Leu). Each of these cell lines displayed high levels of signaling that did not change in response to SHH stimulation (Fig. 2, B to E, and fig. S3, A to G). Pharmacological inhibition of GRK2 kinase activity with cmpd101 or the introduction of loss-of-function mutations in *Grk2* reversed the constitutive signaling seen in *Ptch1*^{-/-} NIH/3T3 cells (Fig. 2B and fig. S3A). Both perturbations also reversed constitutive signaling in Med1-MB cells (fig. S3, H to J), a mouse medulloblastoma cell line that lacks PTCH1 activity and is used to model aspects of Hh-driven human medulloblastomas (29). The IC₅₀ of cmpd101 was very similar between cells that did (4.9 μM) or did not (3.9 μM) contain PTCH1

Fig. 2. GRK2 functions at a step between SMO and Gα_s in the Hh signaling pathway.

(A) The current model for transduction of Hh signals in vertebrates, with positive regulators in green and negative regulators in red. Glioma-associated oncogene (GLI) proteins (yellow) can function as either transcriptional repressors or activators, depending on how they are posttranslationally modified and processed. SMO is thought to reduce protein kinase A (PKA) activity by reducing the amount of GPR161 in primary cilia. Shown to the right of each component are the results from genetic epistasis experiments to establish the order in which the component functions relative to GRK2. SUFU, Suppressor of Fused; PTCH, patched proteins. **(B to E)** Quantification of endogenous *Gli1* mRNA relative to *Gapdh* by qRT-PCR in cells of various genotypes that were exposed to the indicated combinations of SHH and the GRK2 inhibitor cmpd101. In (B), each data point represents mean ± SD (n = 3). In (C) to (E), each data point represents mean ± SD (n = 4). Statistical significance was determined by unpaired Welch's *t* test and depicted as follows: ***P* < 0.01, ****P* < 0.001, *****P* < 0.0001, and *P* > 0.05. n.s., not significant.



Downloaded from <http://stke.sciencemag.org/> on February 20, 2018

(figs. S1A and S3H). Therefore, GRK2 must act downstream of PTCH1 in NIH/3T3 cells.

With respect to SMO, we have previously shown that the constitutive Hh signaling induced by SMO-W539L requires GRK2 (17). Cmpd101 treatment reduced signaling in cells expressing SMO-W539L (Fig. 2C and fig. S3G). Cmpd101 also blocked signaling in cells carrying SMO mutants (D477G and D477R, in which Asp⁴⁷⁷ is mutated to Gly or Arg) that are resistant to the clinically used antagonist vismodegib (Fig. 2C and fig. S3G) (30, 31). These results show that GRK2 functions at the level of SMO or downstream of SMO.

In contrast to the effects on signaling triggered by PTCH1 inactivation or SMO activation, constitutively activated signaling in *Gnas*^{-/-} and *Sufu*^{-/-} cells could not be blocked by cmpd101 or by loss-of-function mutations in *Grk2* (Fig. 2, D and E, and fig. S3, A and B). Together, these results suggest that GRK2 is required for signaling at a step in the Hh pathway from SMO to $G\alpha_s$ (the product of *Gnas* gene) (Fig. 2A). The concordance between the epistatic profile of cmpd101 and the genetic deletion of *Grk2* demonstrates that the effects of this small molecule on the Hh pathway are specific.

To understand how GRK2 may function in NIH/3T3 cells, we took advantage of previous studies that have mapped critical amino acid residues in GRK2 that are required for kinase activity, membrane recruitment, interaction with GPCRs, and binding to G protein subunits (Fig. 3A) (32–35). We generated mutant GRK2 variants that each specifically affects one aspect of GRK2 function and tested their ability to rescue the Hh phenotype observed in *Grk2*^{-/-} cells. Mutations in residues on one face of an N-terminal helix that are known to mediate the interaction of GRK2 with GPCRs failed to rescue Hh reporter

expression in *Grk2*^{-/-} cells (Fig. 3B) (35). In addition, GRK2 function in Hh signaling depended on residues that mediate membrane recruitment through anionic phospholipid binding (Lys⁵⁶⁷ and Arg⁵⁷⁸), but not on residues implicated in binding to the $G\beta\gamma$ complex (Arg⁵⁸⁷) or to $G\alpha_q$ (Asp¹¹⁰) (Fig. 3, A and B). Together with the epistasis analysis above, these data suggest that GRK2 may function in Hh signaling by regulating the activity or abundance of a GPCR other than GPR161 in NIH/3T3 cells. These mutagenesis experiments are also consistent with the possibility that GRK2 regulates SMO itself (because SMO is a GPCR); however, in this latter scenario, GRK2 would have to regulate SMO activity by a mechanism other than altering its ciliary localization, which has been excluded by two independent studies (9, 17).

GRK2/3 are essential for Hh responses in NPCs

Mouse embryos with loss-of-function mutations in *Gpr161* have a defect in patterning of the ventral neural tube, where neural identity is determined by a gradient of SHH ligand secreted by the notochord and the floor plate (Fig. 4A) (8, 36). This well-established morphogenetic activity of Hh ligands can be recapitulated in spinal cord NPCs derived from embryonic stem (ES) cells. As in NIH/3T3 cells, Hh signaling activity can be assessed in NPCs by measuring the induction of GLI1 and PTCH1. However, NPCs also afford a more physiological readout of Hh signaling strength—the adoption of different cell fates that can be assayed by the expression of genes encoding transcription factors that define progenitor identity (Fig. 4A) (25). These transcription factors can be divided into two groups: class I transcription factors that are expressed in the absence of SHH (PAX6) and class II transcription factors whose expression is driven by increasing

Fig. 3. Mapping the residues that are critical for GRK2 function in Hh signaling. (A) Domain structure of GRK2 [adapted from (59)]. RH, regulator of G protein (heterotrimeric guanine nucleotide-binding protein) signaling homology; AGC C-tail, C-terminal extension of the kinase domain reminiscent of PKA, PKG, and PKC; PH, pleckstrin homology. Amino acid residues mutated in our analysis are indicated, along with their previously established effects on GRK2 function. (B) Activation of a luciferase-based Hh reporter gene in *Grk2*^{-/-} NIH/3T3 cells in response to SHH after transient transfection with an empty vector or a vector carrying genes encoding the indicated mutant forms of GRK2—green fluorescent protein (GFP). Each data point represents mean \pm SD ($n = 3$). Statistical significance was determined by unpaired Welch's *t* test and depicted as follows: ** $P < 0.01$.

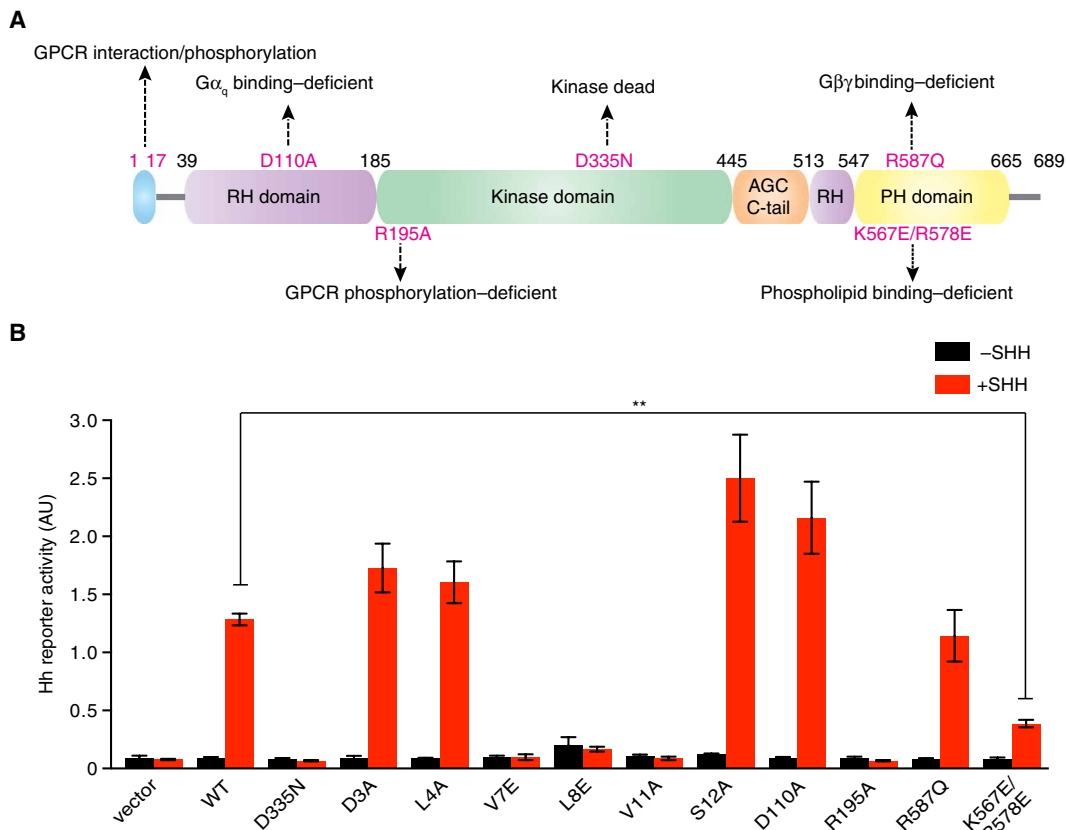
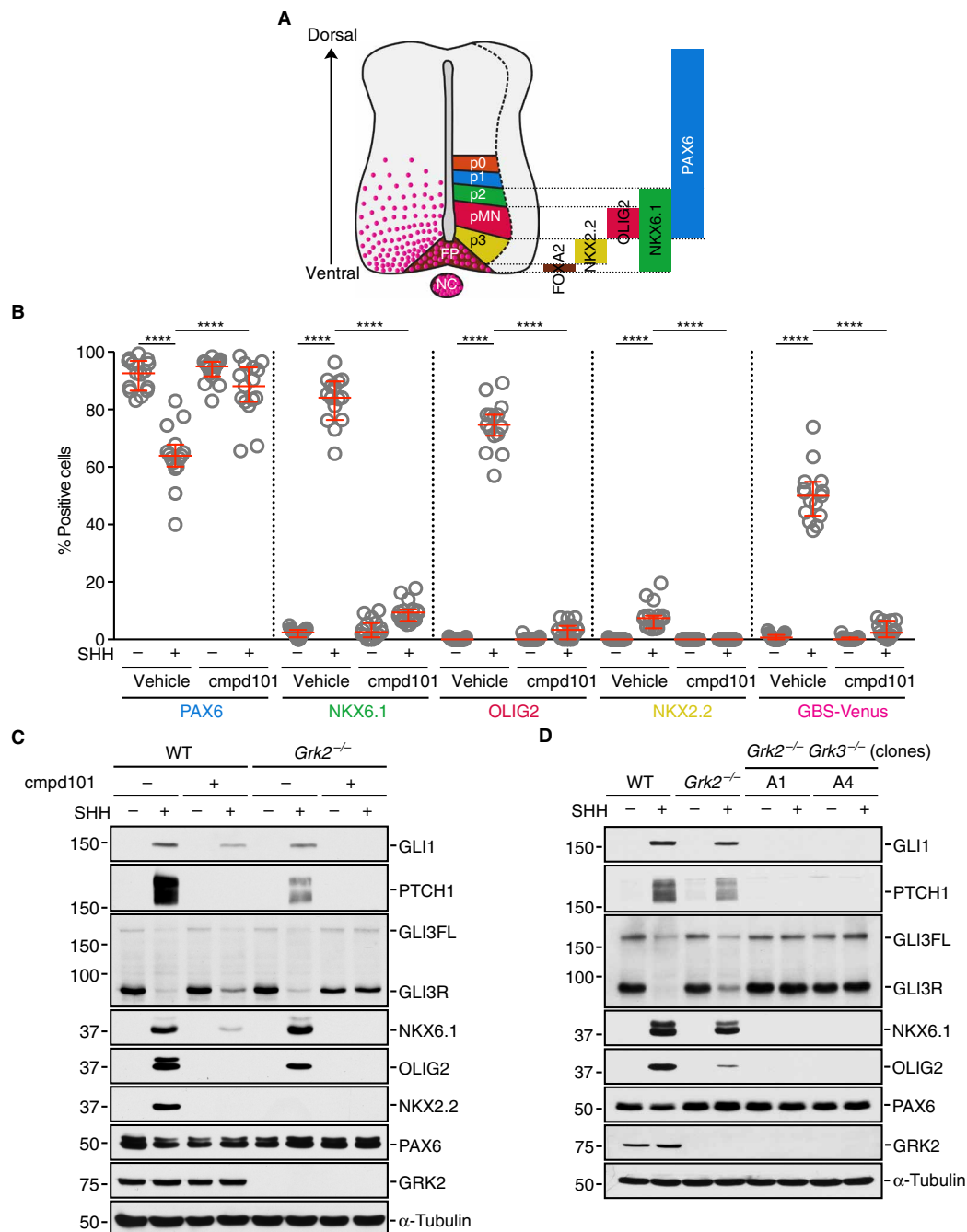


Fig. 4. GRK2 and GRK3 activity is required for spinal neural cell fates that are dependent on all levels of Hh signaling. (A) A schematic of the progenitor domains within the embryonic spinal cord [adapted from (36)]. NC, notochord; FP, floor plate; pMN, motor neuron progenitors; p0, p1, p2, and p3, ventral interneuron progenitors. The progenitor domains are a product of a high-to-low SHH gradient (pink) along the ventral-to-dorsal axis. The bars on the right represent the transcription factors present in each progenitor domain.

(B) Neural progenitor cells (NPCs) carrying the fluorescent Hh reporter GLI binding site (GBS)-Venus were left untreated or treated with SHH, cmpd101, or SHH + cmpd101, followed by immunofluorescence staining to count the percentage of cells positive for transcription factors that define ventral progenitor subtypes summarized in (A). Each data point represents the data from one image of an NPC colony (see fig. S4A) consisting of 100 to 200 cells, and each condition is represented by 15 different colonies. The experiment was repeated twice. Medians with interquartile ranges are shown with statistical significance determined by the Mann-Whitney nonparametric analysis of variance (ANOVA) test and depicted as follows: **** $P < 0.0001$. (C and D) Immunoblots (representative of two independent experiments) showing the indicated proteins in WT, *Grk2*^{-/-} (C), or *Grk2*^{-/-} *Grk3*^{-/-} double-null NPCs (D) treated with the indicated combinations of SHH and cmpd101. Two *Grk2*^{-/-} *Grk3*^{-/-} clonal NPC lines (A1 and A4) are shown in (D), and an independent *Grk2*^{-/-} NPC cell line is shown in fig. S4C.



amounts of Hh signaling (low, NKX6.1; medium, OLIG2; high, NKX2.2; and highest, FOXA2). These transcription factors that define neural identity in the spinal cord can be assessed by (i) measuring their mRNA or protein abundance in bulk NPC cultures or (ii) counting the number of individual cells positive for each transcription factor after immunostaining. In addition, we took advantage of NPCs produced from a mouse ES cell line (mESC) harboring the fluorescent marker Venus under the control of an Hh-responsive promoter carrying multiple GLI binding sites (GBS) from the FOXA2 locus (hereafter called GBS-Venus). Given that GPR161 depletion had no effect on basal signaling in NIH/3T3 cells, we reassessed the roles of GPR161 and GRK2 in NPCs.

When cultured without SHH, NPCs contained low levels of GLI1 and PTCH1 and high levels of PAX6 (Fig. 4, B and C, and fig. S4A). Upon SHH addition, GLI1 and PTCH1 levels increased (Fig. 4C), concomitant with a decrease in PAX6 (Fig. 4, B and C, and fig. S4A). A majority of NPCs differentiated into NKX6.1-positive and OLIG2-positive progenitors, and a smaller fraction into NKX2.2-positive progenitors (Fig. 4, B and C, and fig. S4A).

Because both *Grk2* and *Grk3* are expressed in NPCs (fig. S4D), we tested the dual inhibitor cmpd101 on these cells. Cmpd101 blocked all readouts of Hh signaling activity, including target gene induction, as measured by PTCH1, GLI1 (Fig. 4C), and GBS-Venus expression

(Fig. 4B), and differentiation of progenitor subtypes driven by low (NKX6.1), medium (OLIG2), and high (NKX2.2) levels of signaling (Fig. 4, B and C, and fig. S4A). Thus, GRK2/3 activity is required to mediate all responses to SHH in NPCs.

Unlike NIH/3T3 cells, which only express *Grk2*, NPCs express both *Grk2* and *Grk3* (fig. S4D). NPCs carrying loss-of-function mutations in *Grk2* alone responded to SHH (Fig. 4C and fig. S4, B and C) and remained sensitive to cmpd101 (Fig. 4C and fig. S4A), suggesting that GRK2/3 play redundant roles. Loss-of-function mutations in both *Grk2* and *Grk3* (*Grk2*^{-/-} *Grk3*^{-/-} double-null cells) resulted in a near-complete block in Hh-induced differentiation into ventral cell types, analogous to the effect seen with the dual inhibitor cmpd101 (Fig. 4D). GRK2/3 were functionally redundant because GRK3 could support Hh signaling in NIH/3T3 cells lacking GRK2 (fig. S4E). Redundancy between the paralogous *Grk2* and *Grk3* genes in mice provides a likely explanation for why *Grk2*^{-/-} mice display a much milder Hh signaling phenotype compared to zebrafish *grk2*^{-/-} mutants; the zebrafish genome contains a single gene (named *grk2*) that encodes a protein most similar to mammalian GRK3 (13, 17). In summary, GRK2/3 are required in NPCs for Hh signaling and for Hh-driven differentiation, raising the important question of whether they regulate the pathway through GPR161 in NPCs.

GPR161 inhibits low-level Hh responses and attenuates high-level Hh responses in NPCs

Because GPR161 was originally shown to be a negative regulator of Hh signaling in the neural tube (8), we generated *Gpr161*^{-/-} NPCs (fig. S5A) and tested their differentiation in response to SHH. Consistent with the phenotype observed in the neural tube of *Gpr161*^{-/-} mouse embryos (8), Hh signaling was modestly increased in *Gpr161*^{-/-} NPCs in the absence of Hh ligands (Fig. 5A). This finding was in contrast to the absence of basal Hh pathway activation in NIH/3T3 cells lacking GPR161 (Fig. 1A), highlighting its tissue or cell type specificity. The stronger effect of GPR161 loss on basal Hh signaling in NPCs was not caused by the higher expression of *Gpr161* in NPC cells compared to NIH/3T3 cells (fig. S5B).

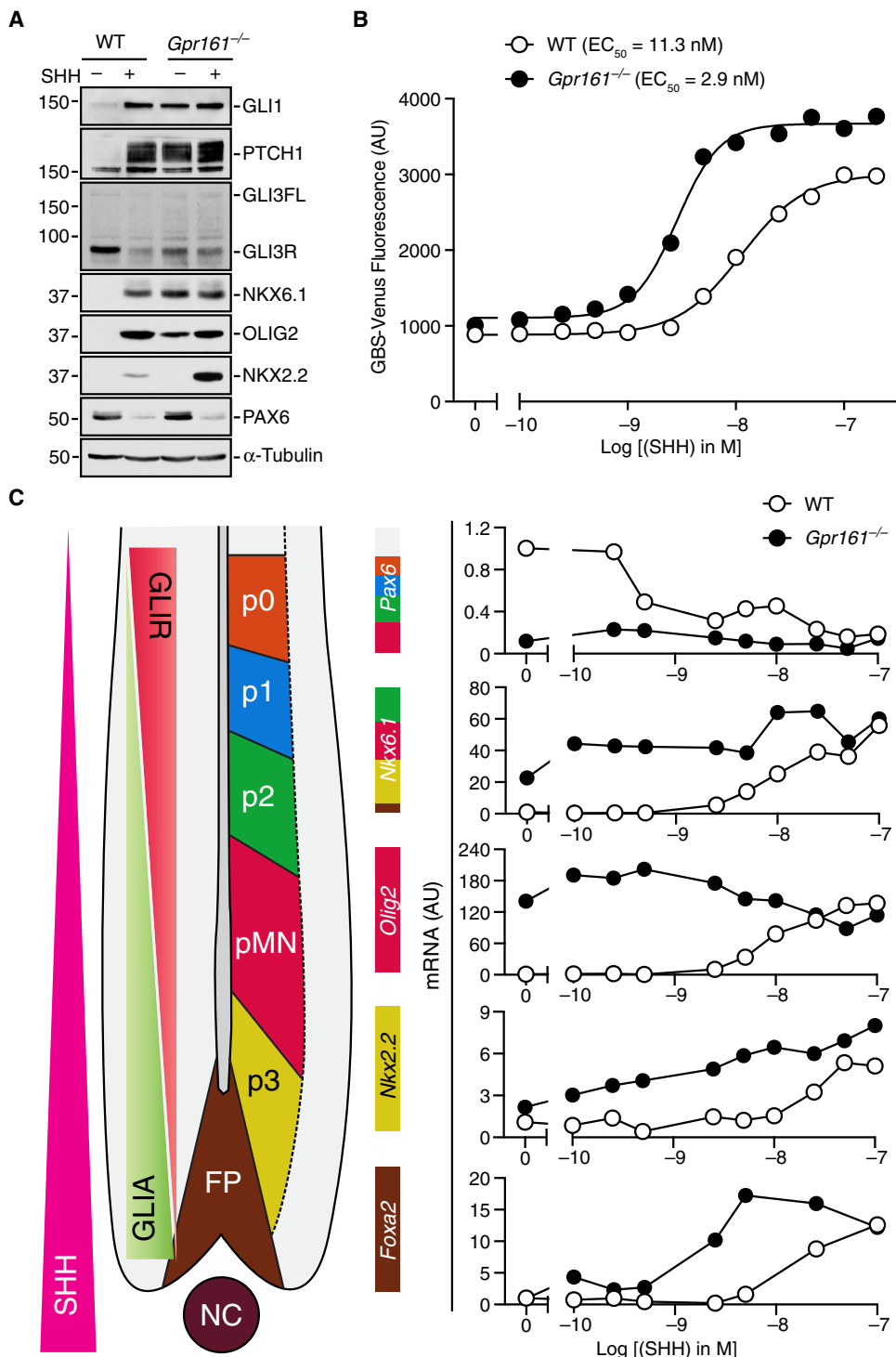


Fig. 5. GPR161 suppresses low-level Hh responses and attenuates high-level Hh responses in NPCs. (A) Hh signaling was assessed ($n = 3$ independent experiments) using immunoblots of extracts from WT and *Gpr161*^{-/-} NPCs left untreated or treated with SHH. (B) Activation of the GBS-Venus reporter in WT or *Gpr161*^{-/-} NPCs treated with increasing concentrations of SHH. Each data point represents median reporter fluorescence calculated from 10,000 cells. (C) A schematic (left) of the progenitor domains within the embryonic spinal cord along with opposing gradients of GLI repressor (GLIR) and GLI activator (GLIA) proteins proposed to establish the spatial pattern of neural subtypes. *Pax6*, *Nkx6.1*, *Olig2*, *Nkx2.2*, and *Foxa2* mRNAs were quantified by qRT-PCR (normalized to *Gapdh*) in WT and *Gpr161*^{-/-} NPCs treated with increasing concentrations of SHH. Immediately to the left of each graph, the domains in the neural tube where each transcription factor is present are depicted as a color code based on the diagram to the left. Each data point represents a mean of three technical replicates. The experiments in (B) and (C) were repeated twice.

In unstimulated *Gpr161*^{-/-} NPCs, we observed an increase in the abundances of GLI1 and PTCH1 and a reduction in GLI3R (Fig. 5A). GLI3 processing into the GLI3R fragment depends on direct PKA-mediated phosphorylation; hence, loss of GPR161, a $G\alpha_s$ -coupled receptor, could prevent GLI3R production by decreasing cAMP levels and PKA activity (2, 8). A predicted consequence of GLI3R loss is the derepression of markers responsive to low-level Hh signals (23, 37). The analysis of markers of ventral neural progenitor subtypes revealed low-level activation of Hh signaling. Most NPCs lacking *Gpr161* contained NKX6.1, driven by the lowest levels of Hh signaling (Fig. 5A and fig. S5C), whereas wild-type cells differentiated predominantly into PAX6-positive NPCs. However, a smaller fraction were positive for OLIG2, the production of which is dependent on intermediate-level Hh signaling, and very few were positive for NKX2.2, which requires high levels of Hh signaling (Fig. 5A and fig. S6A). The basal level of the GBS-Venus reporter fluorescence, which is driven by GLI1 binding sites from the *Foxa2* promoter and responsive to the highest levels of Hh signaling, was not increased in *Gpr161*^{-/-} NPCs compared to wild-type NPCs (Fig. 5B). However, analogous to *Gpr161*^{-/-} NIH/3T3 cells, *Gpr161*^{-/-} NPCs were three- to fourfold more sensitive to SHH (EC₅₀ = 2.9 nM) compared to wild-type cells (EC₅₀ = 11.3 nM) (Fig. 5B).

To clearly understand the effects of GPR161 loss on Hh-driven neural progenitor specification, we simultaneously measured mRNA abundances for a panel of five markers known to be driven by various levels of Hh signaling in NPC cultures treated with increasing doses of SHH, allowing us to construct detailed SHH dose-response curves for each of the markers in both wild-type and *Gpr161*^{-/-} NPCs (Fig. 5C). The loss of GPR161 led to the SHH-independent expression of *Nkx6.1* and *Olig2*, progenitor subtype markers repressed by GLI3R, which, in turn, is inhibited by low-level Hh signals (Fig. 5C). In contrast, *Nkx2.2* and *Foxa2*, markers that depend on high-level Hh signals and GLI2 activator function (GLI2A), were not induced in untreated *Gpr161*^{-/-} NPCs (Fig. 5C). Instead, reminiscent of the effect of GPR161 loss in NIH/3T3 cells, the SHH dose-response curves for the induction of NKX2.2 and FOXA2 were shifted to the left (Fig. 5C). Thus, the loss of GPR161 sensitized cells to Hh ligands, consistent with the ventralized patterning observed in the neural tube in *Gpr161*^{-/-} embryos (8).

Is the activity of either GRK2/3 or SMO required for Hh signaling in the absence of GPR161 in NPCs, like it is in NIH/3T3 cells? GPR161 is considered epistatic to both SMO and GRK2, predicting that neither should be required for signaling in *Gpr161*^{-/-} cells (8, 9). In agreement with this view, the SHH-independent, constitutive signaling activity seen in *Gpr161*^{-/-} NPCs was largely unaffected by cmpd101 and cyclopamine. In the absence of SHH, the increase in NKX6.1- and OLIG2-positive NPCs could not be prevented by pharmacologically inhibiting either SMO or GRK2 (Fig. 6, A to D, and fig. S6, A and B). This is consistent with the hypothesis that differentiation into NKX6.1- or OLIG2-positive progenitor subtypes was likely to be driven by the loss of GLI3R in *Gpr161*^{-/-} NPCs (Fig. 5A). The increased expression of both *Nkx6.1* and *Olig2* observed in response to SHH in *Gpr161*^{-/-} cells could be prevented by SMO inhibition with cyclopamine, but not by cmpd101, perhaps because GRK2/3 activity could not be completely inhibited by cmpd101 or because it was not required under these conditions.

In striking contrast, both cmpd101 and cyclopamine inhibited SHH-induced, high-level Hh signaling in *Gpr161*^{-/-} NPCs, resulting in a marked decrease in the specification of NKX2.2- and GBS-Venus-

positive cells (Fig. 6, A to D, and fig. S6, A and B). Thus, GRK2/3 and SMO must play roles independent of GPR161 in transducing high-level Hh signals, which are presumably mediated predominantly by GLI2A. Together, our analysis in cultured NPCs resolves a paradoxical observation in the developing neural tube of mouse embryos: The induction of NKX6.1- and OLIG2-positive progenitors in *Gpr161*^{-/-} was independent of SMO activity, but the induction of FOXA2 (requiring high level of Hh signaling) remained dependent on SMO activity (8).

In summary, GPR161 and GRK2 appear to be regulating low- and high-level Hh responses in NPCs through apparently distinct mechanisms. GPR161 suppresses low-level Hh responses but only attenuates high-level Hh responses. Although GRK2 activity is essential for all Hh responses, it functions through GPR161 only to regulate low-level (but not high-level) Hh signaling. Thus, low- and high-level responses to the SHH morphogen may be mediated by distinct molecular pathways.

GRK2/3 are required for Hh signaling through a $G\alpha_s$ -dependent pathway

Our work in NIH/3T3 cells demonstrated that GRK2 was dispensable for Hh signaling in the absence of $G\alpha_s$ (Fig. 2D) and also provided evidence that an alternative GPCR (other than GPR161) may mediate the effect of GRK2 on Hh signaling (Fig. 1A). Thus, high-level, GRK2-mediated responses in NPCs, which do not depend on GPR161, may also be regulated by an alternative $G\alpha_s$ -coupled GPCR. Elimination of $G\alpha_s$ from NPCs increased the abundance of both NKX2.2 and FOXA2, which require the highest levels of Hh signaling (Fig. 7A and fig. S7) and were not induced by the loss of *Gpr161* (Fig. 5, A and B). Cmpd101 did not inhibit Hh signaling in cells lacking $G\alpha_s$ (Fig. 7A). Therefore, GRK2 appears to function upstream of $G\alpha_s$ in NPCs, as it does in NIH/3T3 cells, raising the possibility that Hh signaling can be regulated by $G\alpha_s$ -coupled GPCRs other than GPR161. The higher activation of Hh signaling observed in both mouse embryos and cultured cells depleted of $G\alpha_s$ also suggests the involvement of alternative $G\alpha_s$ -coupled GPCRs.

DISCUSSION

We used genetic and pharmacological approaches in two Hh-responsive cell culture systems to dissect the epistatic relationships between GRK2, GPR161, and $G\alpha_s$ in Hh signaling. Our results highlight the importance of distinguishing between negative regulators and attenuators of signaling pathways. Negative regulators, such as SUFU, PTCH1, and $G\alpha_s$, keep the pathway off in the absence of ligand. Their loss leads to constitutive activation of the pathway in the absence of ligand, and they must be antagonized to allow signal propagation to the nucleus. In contrast, attenuators are not essential to signal transduction but may function as components of control systems (such as feedback loops) that dampen signaling by limiting ligand potency or efficacy. Our results show that GPR161 functions as an attenuator of Hh signaling in NIH/3T3 cells and of high-level Hh signals in NPCs. In these contexts, the loss of GPR161 does not lead to spontaneous activation of the pathway but, instead, increases the sensitivity to SHH, with signaling remaining dependent on SMO. However, consistent with previous reports, GPR161 functions as a bona fide negative regulator of low-level Hh responses in NPCs. On the other hand, GRK2 and $G\alpha_s$ were clearly positive and negative regulators, respectively, of signaling across the full range of Hh responses in both fibroblasts and

NPCs, suggesting both GPR161-dependent and GPR161-independent roles for these regulators. Because SHH is a morphogen, the shape of the SHH dose-response curve is predicted to have an effect on tissue pat-

tern. Genes like *Gpr161* may regulate patterning in a unique way, functioning by shaping the sensitivity to morphogens rather than by acting as simple positive or negative regulators of signal propagation.

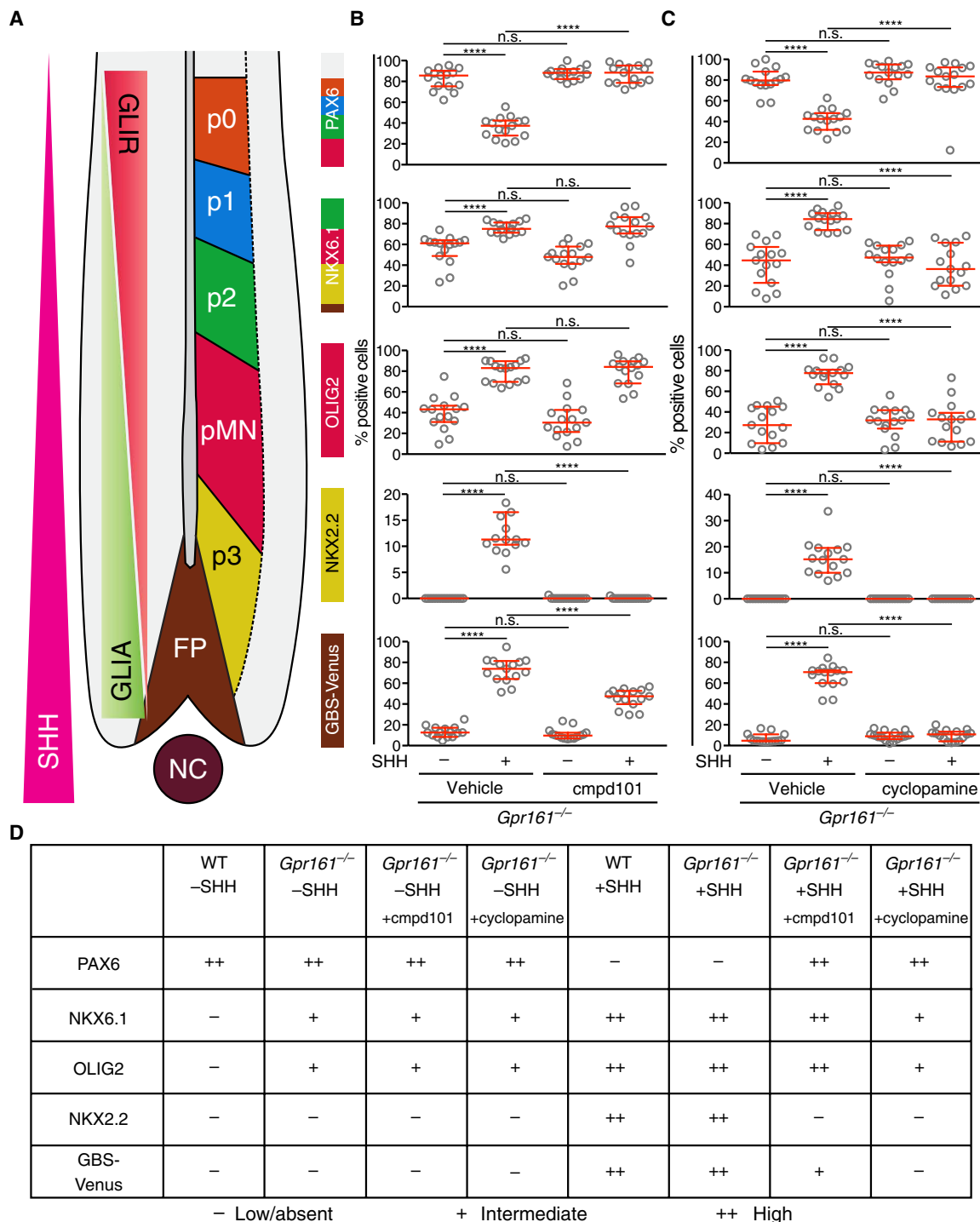


Fig. 6. GRK2 and SMO are required for high-level Hh responses in *Gpr161*^{-/-} NPCs. (A) A schematic of the progenitor domains, with reciprocal GLIR and GLIA domains, as previously shown in Fig.5C. (B and C) The percentage of cells containing progenitor subtype markers (NKX6.1, OLIG2, NKX2.2, and GBS-Venus) with or without SHH exposure in *Gpr161*^{-/-} NPCs assessed at 48 hours after inhibition of GRK2/3 with cmpd101 (B) or inhibition of SMO with cyclopamine (C). Each data point represents the data from one image of an NPC colony (see fig. S6A) consisting of 100 to 200 cells, and each condition is represented by 15 different colonies. The experiment was repeated twice. Medians with interquartile ranges are shown with statistical significance determined by the Mann-Whitney nonparametric ANOVA test and depicted as follows: *****P* < 0.0001 and *P* > 0.05. (D) Summary of the effect of GRK2 and SMO inhibitors on the differentiation of WT and *Gpr161*^{-/-} NPCs.

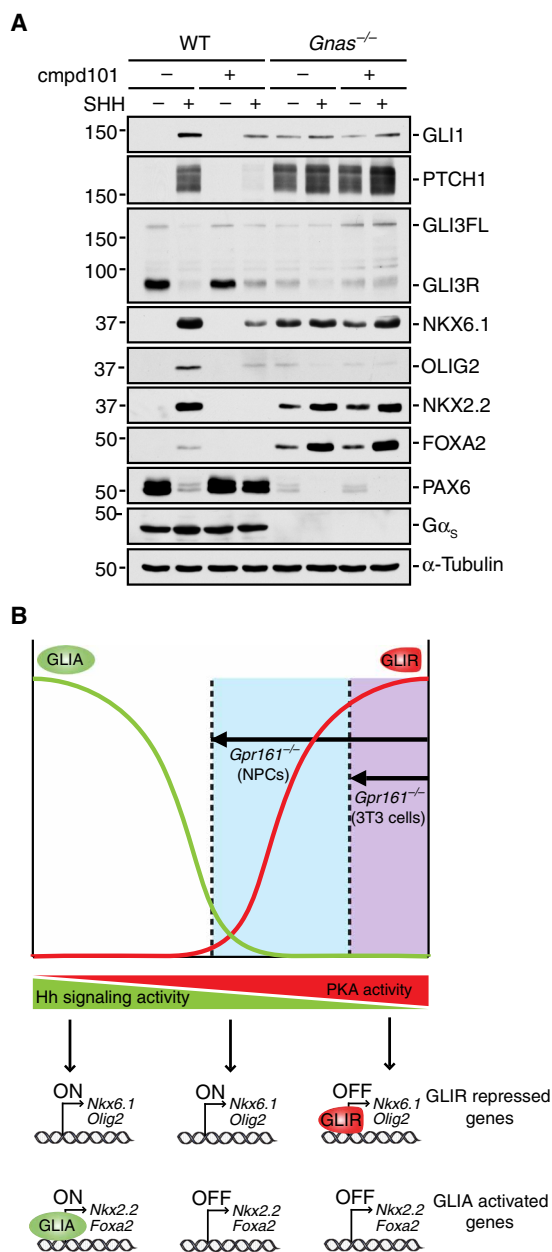


Fig. 7. $G\alpha_s$ negatively regulates all levels of Hh signaling in NPCs. (A) Immunoblot (representative of three independent experiments) showing the effect of GRK2/3 inhibition (by cmpd101) on SHH-induced responses in WT and *Gnas*^{-/-} NPCs. FOXA2 abundance is driven by the highest level of Hh signaling during neural tube development and, hence, can be considered a marker of maximal Hh signaling in this system. (B) A model for the different consequences of GPR161 loss in NIH/3T3 cells and NPCs. Decreasing PKA activity drives increasing levels of signaling, first by preventing GLIR formation and subsequently by allowing formation of GLIA. We speculate that the decrease in PKA activity (arrows) produced by the loss of GPR161 is greater in NPCs compared to NIH/3T3 cells (top). In NPCs only, this decrease in PKA activity drops below the threshold required for the biogenesis of GLI3R and consequently allows for the adoption of cell fates (bottom); NKX6.1- and OLIG2-positive cells repressed by GLI3R in the basal state. In both NPCs and NIH/3T3 cells, the lowered PKA activity sensitizes cells to SHH-induced responses, shifting the SHH dose-response curve to the left.

How could GPR161 have distinct effects on Hh signaling in NPCs compared to NIH/3T3 cells? We favor a model that builds on the previous observation that Hh responsiveness is exquisitely sensitive to the amount of cellular PKA activity (5). Increasing PKA activity leads to a progressive loss in cellular responsiveness to SHH (Fig. 7B). PKA directly phosphorylates and regulates the transcriptional activity of the bifunctional GLI proteins, which can exist either as transcriptional repressors (GLIR) or activators (GLIA). PKA blocks GLI transcriptional activity in a graded manner using a multisite phosphorylation code: Phosphorylation at a group of four residues promotes the proteolytic conversion of GLIs into GLIRs; however, the phosphorylation of an additional set of two residues is required to fully block GLIA (6). SHH can independently prevent GLIR formation and promote GLIA formation by controlling this phosphorylation code.

Given that cellular PKA activity is a central determinant of signaling strength, we propose that the balance between the activity of $G\alpha_s$ -coupled GPCRs (which would raise cAMP levels and, hence, PKA activity) and the activity of $G\alpha_i$ -coupled GPCRs (which would reduce cAMP levels and, hence, PKA activity) may set the sensitivity of target cells to Hh ligands in a tissue-specific or cell type-specific manner. Thus, the different effects of GPR161 on Hh signaling in NIH/3T3 cells and NPCs may be explained by cell type-specific effects on PKA activity (Fig. 7B). In NPCs (but not in NIH/3T3 cells), the decline in PKA activity when GPR161 is eliminated drops below the threshold for GLI3R production, leading to activation of differentiation programs that depend on low- and medium-level Hh responses (Fig. 7B). However, in both NPCs and NIH/3T3 cells, reduced PKA activity caused by GPR161 loss results in increased sensitivity to Hh ligands, manifested as a leftward shift of the SHH dose-response curve.

This model can also explain how the loss of GPR161 in NPCs can have apparently distinct effects on high- and low-level Hh responses. The spontaneous differentiation phenotype of *Gpr161*^{-/-} NPCs is likely to be explained by the loss of GLI3R in these cells in the absence of any Hh ligands (Fig. 7B) (8). The production of NKX6.1 and OLIG2, the transcription factors found in NPCs lacking GPR161, is known to be repressed by GLI3R in the neural tube (25, 37, 38). However, the loss of GPR161 may not be sufficient to fully activate GLI2A, which drives the production of NKX2.2 and FOXA2 in response to high-level Hh signals in the ventral-most domains of the neural tube (Fig. 7B). These results are consistent with the observation that neural tube patterning defects in mouse embryos lacking GPR161 are more severe than those lacking GLI3, but less severe than those lacking other negative regulators like PKA and $G\alpha_s$ (18, 19, 21, 22).

In comparison to GPR161, GRK2 regulates the production of transcription factors that depend on both GLI3R and GLI2A for their expression. The effect of GRK2 on GLI3R-regulated genes depends on GPR161 because GRK2 activity is dispensable for the production of NKX6.1 and OLIG2 in *Gpr161*^{-/-} NPCs (Fig. 6, A and B). However, even in *Gpr161*^{-/-} NPCs, GRK2 is still necessary for SHH to induce transcription factors that depend on GLI2A (Fig. 6, B and D, and fig. S6A), demonstrating a GPR161-independent role for GRK2 in regulating high-level Hh responses. Although the mechanism by which GRK2/3 regulate GPR161-independent signaling remains to be determined, it may involve either (i) the regulation of an alternate $G\alpha_s$ -coupled GPCR or (ii) the regulation of high-level signaling by SMO itself, which does not couple to $G\alpha_s$.

A key unresolved question is whether $G\alpha_s$ -coupled GPCRs, including GPR161, are directly regulated by Hh ligands or whether they simply set the basal PKA activity level in cells that then modulates

signaling strength or sensitivity. It has been challenging to observe changes in PKA enzymatic activity or cAMP levels in response to Hh ligands, although it is possible that such changes are restricted to a microdomain or to the cilium (39, 40). A direct regulatory role has been suggested on the basis of the observation that GPR161 is cleared from the ciliary membrane in response to SHH or SMO agonists (8, 9). However, our observations in NIH/3T3 cells show that ciliary trafficking changes, even when correlated with signal activation, may not play a functional role. Other components that could be regulated by SMO include $G\alpha_i$ proteins [which reduce PKA activity and can be directly activated by SMO (41–45)], GRK2, or the GLI-SUFU complex. NPCs lacking $G\alpha_s$, despite displaying very high levels of Hh target gene transcription, remain responsive to SHH, suggesting that SMO regulates a process that is at least partially independent of $G\alpha_s$ and, hence, of the GPCRs that couple to $G\alpha_s$ (Fig. 7A).

We conclude with a few comments about the therapeutic relevance of our findings. SMO antagonists are Food and Drug Administration–approved drugs used in advanced basal cell cancers. As with many other protein-targeted therapies, resistance has been observed in the clinic, predominantly caused by mutations in SMO itself that prevent drug binding or drug activity (31, 46, 47). Thus, Hh inhibitors that act downstream of SMO are of interest (48). GRK2/3 inhibitors, which have been explored largely for their potential utility in heart failure, should be effective in blocking signaling mediated by drug-resistant mutants of SMO (fig. S3G).

MATERIALS AND METHODS

Cell culture

F1p-In-3T3 (a subline of NIH/3T3 cells) and 293FT cell lines were purchased from Life Technologies. The Med1-MB cell line was a gift from M. P. Scott (Stanford University). Stable cell lines expressing SMO mutants in the background of *Smo*^{-/-} MEFs were previously described (49). Stable F1p-In-3T3 cell lines expressing tagged GRK2 [C-terminal green fluorescent protein (GFP) or 1D4 tag], PTCH1 (C-terminal APEX2-1D4 tag), $G\alpha_s$ (internal GFP tag), GPR161 (C-terminal YFP-FLAG tag), and SUFU (C-terminal APEX-1D4 tag) were generated as previously described (50). All the above-mentioned cell lines were cultured in Dulbecco's modified Eagle's medium (DMEM) containing high glucose (Thermo Fisher Scientific) and supplemented with 10% fetal bovine serum (FBS) (Atlanta Biologicals), 1 mM sodium pyruvate (Gibco), 2 mM L-glutamine (Gemini Biosciences), 1× MEM nonessential amino acids solution (Gibco), penicillin (40 U/ml), and streptomycin (40 µg/ml) (Gemini Biosciences) in a humidified atmosphere containing 5% CO₂ at 37°C. To induce ciliation, cells were grown to confluence in DMEM containing 10% FBS and then switched to medium containing 0.5% FBS for 24 hours. Treatment with Hh pathway agonists [25 nM SHH and 200 nM SMO agonist (SAG)], antagonists (200 nM SANT-1, 5 µM cyclopamine, and 1 µM vismodegib), and GRK2/3 inhibitor (25 µM cmpd101) was either done for 4 hours after serum starvation (immunofluorescence staining) or included during the 24-hour serum starvation step [quantitative reverse transcription polymerase chain reaction (qRT-PCR); except for figs. S1A and S3H, in which treatment was 4 hours], Western blotting, and reporter assays].

Neural progenitor differentiation

A stable GBS-Venus reporter line (DVI2) was generated using HM1 mESCs. The 8xGBS-H2B::Venus Shh reporter was cloned into the

hypoxanthine-guanine phosphoribosyltransferase (HPRT)–targeting vector, pSKB1 (51). The HPRT-8xGBS-H2B::Venus construct was integrated into the HPRT locus of HM1 cells using nucleofection. Positive clones were selected for 8 days using hypoxanthine aminopterin thymidine (HAT) medium (Sigma-Aldrich). Single colonies were expanded on feeder layers in ES cell medium with leukemia inhibitory factor (LIF) and characterized by PCR. To prepare the dishes for mESC maintenance, we plated feeders onto dishes coated with 0.1% gelatin (Sigma-Aldrich) overnight. The mESCs were cultured with feeders in mESC media [DMEM containing high glucose, 15% Optima FBS (Atlanta Biologicals), 1× MEM nonessential amino acids, 1% penicillin/streptomycin, 2 mM L-glutamine, 1% EmbryoMax nucleosides (Millipore), 55 µM 2-mercaptoethanol (Gibco), and ESGRO LIF (1000 U/ml; Millipore)]. The mESCs were differentiated into spinal neural progenitors using a previously described protocol with minor modifications (52). Briefly, for this differentiation, the feeders were first removed from the mESCs. This was achieved by lifting the cells off the maintenance plates with 0.25% trypsin/EDTA and incubating the cells on 10-cm tissue culture plates for two short successive periods (20 min each). To induce neural differentiation, we plated the cells onto either gelatin-coated glass coverslips (12 mm in diameter, placed in a 24-well plate) at a density of 24×10^3 cells per coverslip or gelatin-coated CellBIND plates (Corning) at a density of 60×10^3 cells per six well or 100×10^3 cells per 10-cm plate. For the differentiation, cells were plated in N2B27 media [DMEM F12 (Gibco) and Neurobasal Medium (Gibco) (1:1 ratio) supplemented with N-2 Supplement (Gibco), B-27 Supplement (Gibco), 1% penicillin/streptomycin (Gemini Bio-Products), 2 mM L-glutamine (Gemini Bio-Products), bovine serum albumin (40 µg/ml; Sigma), and 55 µM 2-mercaptoethanol (Gibco)] with varying components. On day 0 (plating day) and day 1, cells were cultured in N2B27 with basic fibroblast growth factor (bFGF) (10 ng/ml; R&D Systems). On day 2, the cells were cultured in N2B27 with bFGF (10 ng/ml; R&D Systems) and 5 µM CHIR99021 (Axon). On day 3, the cells were cultured in N2B27 containing the following components: retinoic acid (RA) (100 nM; Sigma-Aldrich), RA + SHH (25 nM), RA + cmpd101 (5 µM), RA + SHH + cmpd101, RA + cyclopamine (5 µM), RA + SHH + cyclopamine, RA + SANT-1 (200 nM), or RA + SHH + SANT-1. On day 4, the cell culture media were replenished with fresh media containing the same components. On day 5, the cells were rinsed with phosphate-buffered saline (PBS) and fixed with 4% paraformaldehyde (PFA) for further analysis using immunohistochemistry, or the protein was extracted for Western blot analysis.

Constructs

Mouse *Grk2* and *Grk3* were tagged with a C-terminal GFP or 1D4 and cloned into the pEF5/FRT/V5-DEST vector (Life Technologies). *Grk2* mutants were generated by site-directed mutagenesis. Mouse *Gpr161* was tagged with a dual YFP-FLAG tag and cloned into the pEF5/FRT/V5-DEST vector. Mouse *Ptch1* and *Sufu* were tagged with a dual APEX2-1D4 tag and cloned into the pEF5/FRT/V5-DEST vector. Rat *Gnas* with an internal GFP tag (53) was cloned into the pEF5/FRT/V5-DEST vector.

Reagents and antibodies

Recombinant SHH was generated as previously described (54). The following chemicals were used: SAG (Enzo Life Sciences), SANT-1 (EMD Millipore), cyclopamine and vismodegib (LC Laboratories), cmpd101 (heliobio), and puromycin (Sigma-Aldrich). The following primary antibodies were used: mouse anti-GRK2 (1:500; sc-13143,

Santa Cruz Biotechnology), mouse anti-GLI1 (1:500; 2643, Cell Signaling Technology), goat anti-GLI3 (1:200; AF3690, R&D Systems), rabbit anti-p38 (1:2000; ab7952, Abcam), mouse anti-G α s (1:200; ac-135914, Santa Cruz Biotechnology), goat anti-GFP (1:500; 600-101-215, Rockland), rabbit anti-GFP (1:5000; NB600-308, Novus Biologicals), mouse anti-1D4 (1:5000; The University of British Columbia), mouse anti- α -tubulin (1:10,000; T6199, Sigma-Aldrich), mouse anti-acetylated tubulin (1:10,000; T6793, Sigma-Aldrich), mouse anti-NKX2.2 (1:100; 74.5A5, Developmental Studies Hybridoma Bank), mouse anti-NKX6.1 (1:100; F55A10, Developmental Studies Hybridoma Bank), rabbit anti-PAX6 (1:1000; AB2237, EMD Millipore), and mouse anti-FOXA2 (1:100; 4C7, Developmental Studies Hybridoma Bank). Rabbit polyclonal antibodies recognizing PTCH1, SMO, and SUFU have been described previously (5, 55). Rabbit anti-GPR161 (1:150) and guinea pig anti-OLIG2 (1:20,000) antibodies have been described previously (8, 56). Secondary antibodies conjugated to horseradish peroxidase or Alexa Fluor dyes were obtained from Jackson Laboratories and Thermo Fisher Scientific, respectively. All other reagents and chemicals were of the highest quality available.

CRISPR/Cas9-mediated gene editing in 3T3 and NPCs

Flp-In-3T3 *Grk2*^{-/-}, *Ptch1*^{-/-}, *Gnas*^{-/-}, *Sufu*^{-/-}, *Gpr161*^{-/-}, *Ptch1*^{-/-} *Grk2*^{-/-}, *Gnas*^{-/-} *Grk2*^{-/-}, and *Sufu*^{-/-} *Grk2*^{-/-} cells were generated by CRISPR-Cas9 gene editing technology as previously described (57). Briefly, guide RNA sequences targeting *Grk2* (5'-ctggaacagctcccctcgg-3'), *Gnas* (5'-gaccgaggaccagcgaacg-3'), and *Gpr161* [5'-ggtgac-tagctccatccgga-3' (pool 1), 5'-gtctgcccctatttgg-3' (pool 2), 5'-gat-gaccaacaaatagggg-3' (pool 3), and 5'-ctacggttctctcggg-3' (pool 4)] were cloned into lentiCRISPR v2 plasmid (Addgene #52961). Lentivirus was generated in 293FT cells by transfecting 3,000,000 cells with 8 μ g of lentiCRISPR v2 plasmid, 4 μ g of pCMV-VSV-G (58) plasmid (Addgene #8454), 4 μ g of psPAX2 packaging plasmid (Addgene #12260), and 48 μ l of polyethylenimine (1 mg/ml; Polysciences). The culture medium was changed 14 hours after transfection, and the lentivirus was collected after 48 hours by a brief spin at 400g, followed by a filtration through a 0.45- μ m low-protein binding membrane (Pall Corporation). Flp-In-3T3 cells were transduced with the lentivirus and selected with puromycin containing DMEM (2 μ g/ml) for 10 days. Single cells were sorted into a 96-well plate using FACSAria II (BD Biosciences). Multiple single cell-derived clones (except for *Gpr161*, for which pooled knockout cell lines were used) were analyzed by Western blotting to obtain clones with complete depletion of the gene product. To generate *Ptch1*^{-/-} and *Sufu*^{-/-} cells, we cloned guide RNA sequences targeting *Ptch1* (5'-agctaactcagaccaacg-3') and *Sufu* (5'-gcgggacactctcctaga-3') into pX330-U6-Chimeric_BB-CBh-hSpCas9 (PX330, Addgene #42230). Flp-In-3T3 cells were transiently transfected with the CRISPR plasmid along with a control GFP plasmid using X-tremeGENE 9 (Roche), and GFP-positive single cells were sorted into a 96-well plate using FACSAria II. Single cell-derived null clones were obtained by Western blotting. Knockout of *Grk2* in the background of *Ptch1*^{-/-}, *Gnas*^{-/-}, and *Sufu*^{-/-} was achieved using the lentiCRISPR v2 plasmid expressing the guide RNA targeting *Grk2*, with the exception of *Gnas*^{-/-} cells in which a blastocidin resistance cassette containing lentiCRISPR v2 plasmid was used [provided by H. Ho, University of California (UC) Davis]. *Gpr161*^{-/-}, *Grk2*^{-/-}, *Grk2*^{-/-} *Grk3*^{-/-}, and *Gnas*^{-/-} NPCs were generated using CRISPR-Cas9 gene editing technology. Briefly, guide RNA sequences targeting *Gpr161* (5'-ggtgactagctccatccgga-3'), *Grk2* (5'-ctggaacagctcccctcgg-3'), *Grk3* (dual guides: 5'-attctgtcagtggaagaacg-3' and 5'-gct-

gtctctcgtagcactg-3'), and *Gnas* (5'-cgtaaaccattaacatgc-3' for clone C1; dual guides: 5'-gtgtgcccgcccaactatc-3' and 5'-gtgggtagcagcgaactc-3' for clones C3, C6, and D5) were cloned into the plasmid PX459 (Addgene #48139). These guide constructs were electroporated into GBS-Venus mESCs using the Lonza nucleofection system (Nucleofector 2b Device using the program A-023 and Lonza Cell Nucleofector Kit #VAPH-1001). mESCs were cultured under feeder-free conditions in 2i media [DMEM F12 (Gibco) and Neurobasal Medium (Gibco) (1:1 ratio) supplemented with N-2 Supplement (Gibco), B-27 Supplement (Gibco), 1% penicillin/streptomycin (Gemini Bio-Products), 2 mM L-glutamine (Gemini Bio-Products), bovine serum albumin (40 μ g/ml; Sigma), 55 μ M 2-mercaptoethanol (Gibco), 5 μ M CHIR99021 (Axon), 1 μ M PD 98059 (Axon), and ESGRO LIF (1000 U/ml; Millipore)]. Antibiotic selection was performed 24 hours after nucleofection in 2i media containing puromycin (1.5 μ g/ml) for 48 hours. About 1 week after selection, individual mESC colonies were manually picked and expanded, and the genomic DNA was collected using the QuickExtract DNA Extraction Solution (Epicentre). The region surrounding the guide target was PCR-amplified and sequenced to determine whether nonhomologous end joining resulted in a nonsense or frameshift mutation.

Real-time qRT-PCR

Real-time qRT-PCR in Flp-In 3T3 cells was performed using the Power SYBR Green Cells-to-CT Kit (Thermo Fisher Scientific) on the QuantStudio 5 Real-Time PCR System (Applied Biosystems) with custom-designed primers for *Gli1* (forward primer: 5'-ccaagcaacttatgtcagg-3' and reverse primer: 5'-agcccgtcttcttgaattga-3'), *Grk2* (forward primer: 5'-cgactctactgttccc-3' and reverse primer: 5'-tctggatcacatcacactg-3'), *Grk3* (forward primer: 5'-ctggacaacgaagagatagg-3' and reverse primer: 5'-tgtagcgtcacctgttc-3'), *Gpr161* (forward primer: 5'-ctcacgcttgggtcattg-3' and reverse primer: 5'-gagccagatgtagacgagc-3'), and glyceraldehyde-3-phosphate dehydrogenase (*Gapdh*) (forward primer: 5'-agtggcaaatggagatt-3' and reverse primer: 5'-gtggatgcatcactggaaca-3'). For NPCs, RNA extraction and complementary DNA synthesis were done using TRIzol reagent (Life Technologies) and iScript Reverse transcription supermix (Bio-Rad) following the manufacturer's instructions. The following primers were used for real-time qRT-PCR: *Nkx6.1* (forward primer: 5'-cccggatgtagcagagt-3' and reverse primer: 5'-gaactgggtctggtgtgt-3'), *Olig2* (forward primer: 5'-agaccgagccaacaccag-3' and reverse primer: 5'-aagctctcgaatgacctctt-3'), *Nkx2.2* (forward primer: 5'-cagctcatcctctcac-3' and reverse primer: 5'-tcactccatccttctcc-3'), *Foxa2* (forward primer: 5'-ggagtgt-actcaggcctatta-3' and reverse primer: 5'-ctccactcagcctctctt-3'), and *Pax6* (forward primer: 5'-accggcagaagatcgtag-3' and reverse primer: 5'-tttgatctgcatgggtct-3'). Transcript levels relative to *Gapdh* were calculated using the $\Delta\Delta C_t$ method.

Western blotting

Whole-cell extracts from Flp-In-3T3, and NPCs were prepared in radioimmunoprecipitation assay lysis buffer [50 mM Tris-HCl (pH 8.0), 150 mM NaCl, 2% NP-40, 0.25% deoxycholate, 0.1% SDS, 1 mM NaF, 1 mM dithiothreitol, 10% glycerol, 1 \times SIGMAFAST protease inhibitor cocktail (Sigma-Aldrich), and 1 \times PhosSTOP (Roche)]. Samples were resuspended in Laemmli buffer, incubated for 30 min at room temperature, and subjected to SDS-polyacrylamide gel electrophoresis. The resolved proteins were transferred onto a nitrocellulose membrane (Bio-Rad) using a wet electroblotting system (Bio-Rad) followed by immunoblotting.

Hh reporter assay

Hh reporter assay was performed as described previously (17). Briefly, wild-type or *Grk2*^{-/-} NIH/3T3 cells were seeded in 96-well plates and transfected after 24 hours using X-tremeGENE 9 (Roche) following the manufacturer's instructions. The transfection mix consisted of 32 ng of firefly luciferase reporter driven by an 8xGli-responsive promoter, 8 ng of a Renilla luciferase reporter driven by a constitutive TK (thymidine kinase) promoter (Promega), and 1 ng of vector control or GRK2/GRK3 construct or 10 ng of GPR161. Forty-eight hours after transfection, confluent cells were serum-starved for 24 hours in the presence of SHH (25 nM) or SAG (100 nM). Reporter activity was measured using the Dual-Luciferase Reporter Kit (Promega) and read on the Synergy H1 Hybrid Multi-Mode Microplate Reader (BioTek). The GLI luciferase-to-Renilla luciferase ratio is reported as "Hh reporter activity."

Immunofluorescence staining and image quantifications

Immunofluorescence staining of YFP-tagged GPR161 and endogenous SMO in Flp-In-3T3 cells was performed as described previously (50). Ciliary GPR161 and SMO quantifications were done as previously described (50). For immunofluorescence staining of NPCs, cells were rinsed once with PBS and fixed in 4% PFA for 10 min at room temperature. After blocking for 30 min at room temperature in antibody blocking solution (1% horse serum and 0.1% Triton X-100 in PBS), primary antibodies were applied overnight at 4°C. Coverslips were rinsed with PBS-T (0.1% Triton X-100 in PBS), and secondary antibodies were applied at room temperature for 1 hour, rinsed with PBS-T, and then mounted in ProLong Diamond Antifade Mountant (Life Technologies). Fluorescent images were collected on a Leica TCS SP8 confocal imaging system equipped with a 40× oil immersion objective and captured using the Leica Application Suite X software. In each experiment, coverslips from each condition were grown, collected, and processed together to ensure uniformity across fixation and staining times. While collecting images, the gain, offset, and laser power settings on the microscope were held constant for each antibody. Fifteen images were taken per condition. To ensure full representation, we acquired z-stacks and performed counts on compressed images. Cell counts were collected using the National Institutes of Health ImageJ software suite with Cell Counter plugin. In total, more than 1500 cells were analyzed per condition, and each experiment was independently conducted at least twice. Representative images were processed equally using Adobe Photoshop and Adobe Illustrator.

Quantification and statistical analysis

In all data panels, representative data from two to four independent experiments are shown. The statistical significance of differences between the *Gli1* mRNA levels or Hh reporter activity between two samples was determined by an unpaired Welch's *t* test, with a post-Bonferroni correction applied to correct for multiple comparisons (grouped by graph). Statistical analysis for differences in ciliary fluorescence intensity (NIH/3T3 cells) or neural differentiation marker positivity (in NPCs) between two groups was evaluated using the Mann-Whitney nonparametric analysis of variance (ANOVA) test, with a Bonferroni correction applied to correct for multiple comparisons (grouped by graph). The statistical tests were performed in consultation with an expert statistician in the Department of Biomedical Data Science in Stanford University School of Medicine.

SUPPLEMENTARY MATERIALS

www.sciencesignaling.org/cgi/content/full/11/516/eaao5749/DC1

Fig. S1. Cmpd101 inhibits Hh signaling in NIH/3T3 cells.

Fig. S2. GRK2 affects the ciliary localization of GPR161 in NIH/3T3 cells.

Fig. S3. GRK2 functions at a step between SMO and $G\alpha_5$ in Hh signaling.

Fig. S4. SHH signaling in NPCs is mediated through GRK2/3.

Fig. S5. GPR161 suppresses NPC differentiation responses that are driven by low-level Hh signals.

Fig. S6. High-level Hh responses in *Gpr161*^{-/-} NPCs depend on GRK2 and SMO.

Fig. S7. $G\alpha_5$ regulates both low-level and high-level Hh responses in NPCs.

Table S1. List of pooled or clonal knockout cell lines generated by CRISPR/Cas9.

REFERENCES AND NOTES

- Dessaud, L. L. Yang, K. Hill, B. Cox, F. Ulloa, A. Ribeiro, A. Mynett, B. G. Novitch, J. Briscoe, Interpretation of the sonic hedgehog morphogen gradient by a temporal adaptation mechanism. *Nature* **450**, 717–720 (2007).
- Wang, J. F. Fallon, P. A. Beachy, Hedgehog-regulated processing of Gli3 produces an anterior/posterior repressor gradient in the developing vertebrate limb. *Cell* **100**, 423–434 (2000).
- Corbit, K. C. Anstad, V. Singla, A. R. Norman, D. Y. R. Stainier, J. F. Reiter, Vertebrate smoothed functions at the primary cilium. *Nature* **437**, 1018–1021 (2005).
- Hui, S. Angers, Gli proteins in development and disease. *Annu. Rev. Cell Dev. Biol.* **27**, 513–537 (2011).
- Humke, E. W. Dorn, L. Milenkovic, M. P. Scott, R. Rohatgi, The output of Hedgehog signaling is controlled by the dynamic association between Suppressor of Fused and the Gli proteins. *Genes Dev.* **24**, 670–682 (2010).
- Niewiadomski, J. H. Kong, R. Ahrends, Y. Ma, E. W. Humke, S. Khan, M. N. Teruel, B. G. Novitch, R. Rohatgi, Gli protein activity is controlled by multisite phosphorylation in vertebrate hedgehog signaling. *Cell Rep.* **6**, 168–181 (2014).
- Tukachinsky, L. V. Lopez, A. Salic, A mechanism for vertebrate Hedgehog signaling: Recruitment to cilia and dissociation of SuFu–Gli protein complexes. *J. Cell Biol.* **191**, 415–428 (2010).
- Mukhopadhyay, X. Wen, N. Ratti, A. Loktev, L. Rangell, S. J. Scales, P. K. Jackson, The ciliary G-protein-coupled receptor Gpr161 negatively regulates the Sonic hedgehog pathway via cAMP signaling. *Cell* **152**, 210–223 (2013).
- Pal, S.-H. Hwang, B. Somatilaka, H. Badgandi, P. K. Jackson, K. DeFea, S. Mukhopadhyay, Smoothed determines β -arrestin-mediated removal of the G protein-coupled receptor Gpr161 from the primary cilium. *J. Cell Biol.* **212**, 861–875 (2016).
- Pitcher, N. J. Freedman, R. J. Lefkowitz, G protein-coupled receptor kinases. *Annu. Rev. Biochem.* **67**, 653–692 (2003).
- Chen, X.-R. Ren, C. D. Nelson, L. S. Barak, J. K. Chen, P. A. Beachy, F. de Sauvage, R. J. Lefkowitz, Activity-dependent internalization of smoothed mediated by β -arrestin 2 and GRK2. *Science* **306**, 2257–2260 (2004).
- Meloni, G. B. Fralish, P. Kelly, A. Salahpour, J. K. Chen, R. J. Wechsler-Reya, R. J. Lefkowitz, M. G. Caron, Smoothed signal transduction is promoted by G protein-coupled receptor kinase 2. *Mol. Cell Biol.* **26**, 7550–7560 (2006).
- Philipp, G. B. Fralish, A. R. Meloni, W. Chen, A. W. MacInnes, L. S. Barak, M. G. Caron, Smoothed signaling in vertebrates is facilitated by a G protein-coupled receptor kinase. *Mol. Biol. Cell* **19**, 5478–5489 (2008).
- Chen, S. Li, C. Tong, Y. Zhao, B. Wang, Y. Liu, J. Jia, J. Jiang, G protein-coupled receptor kinase 2 promotes high-level Hedgehog signaling by regulating the active state of Smo through kinase-dependent and kinase-independent mechanisms in *Drosophila*. *Genes Dev.* **24**, 2054–2067 (2010).
- Chen, N. Sasai, G. Ma, T. Yue, J. Jia, J. Briscoe, J. Jiang, Sonic Hedgehog dependent phosphorylation by CK1 α and GRK2 is required for ciliary accumulation and activation of smoothed. *PLoS Biol.* **9**, e1001083 (2011).
- Evron, T. L. Daigle, M. G. Caron, GRK2: Multiple roles beyond G protein-coupled receptor desensitization. *Trends Pharmacol. Sci.* **33**, 154–164 (2012).
- Zhao, R. T. H. Lee, G. V. Pusapati, A. Iyu, R. Rohatgi, P. W. Ingham, An essential role for Grk2 in Hedgehog signalling downstream of Smoothed. *EMBO Rep.* **17**, 739–752 (2016).
- Regard, D. Malhotra, J. Gvozdenovic-Jeremic, M. Josey, M. Chen, L. S. Weinstein, J. Lu, E. M. Shore, F. S. Kaplan, Y. Yang, Activation of Hedgehog signaling by loss of GNAS causes heterotopic ossification. *Nat. Med.* **19**, 1505–1512 (2013).
- He, L. Zhang, Y. Chen, M. Remke, D. Shih, F. Lu, H. Wang, Y. Deng, Y. Yu, Y. Xia, X. Wu, V. Ramaswamy, T. Hu, F. Wang, W. Zhou, D. K. Burns, S. H. Kim, M. Kool, S. M. Pfister, L. S. Weinstein, S. L. Pomeroy, R. J. Gilbertson, J. B. Rubin, Y. Hou, R. Wechsler-Reya, M. D. Taylor, Q. R. Lu, The G protein α subunit $G\alpha_5$ is a tumor suppressor in Sonic hedgehog-driven medulloblastoma. *Nat. Med.* **20**, 1035–1042 (2014).
- Iglesias-Bartolome, D. Torres, R. Marone, X. Feng, D. Martin, M. Simaan, M. Chen, L. S. Weinstein, S. S. Taylor, A. A. Molinolo, J. S. Gutkind, Inactivation of a $G\alpha_5$ -PKA tumour suppressor pathway in skin stem cells initiates basal-cell carcinogenesis. *Nat. Cell Biol.* **17**, 793–803 (2015).

21. S.-H. Hwang, S. Mukhopadhyay, G-protein-coupled receptors and localized signaling in the primary cilium during ventral neural tube patterning. *Birth Defects Res. A Clin. Mol. Teratol.* **103**, 12–19 (2015).
22. M. Tuson, M. He, K. V. Anderson, Protein kinase A acts at the basal body of the primary cilium to prevent Gli2 activation and ventralization of the mouse neural tube. *Development* **138**, 4921–4930 (2011).
23. M. Persson, D. Stamatakis, P. te Welscher, E. Andersson, J. Böse, U. Rüter, J. Ericson, J. Briscoe, Dorsal-ventral patterning of the spinal cord requires Gli3 transcriptional repressor activity. *Genes Dev.* **16**, 2865–2878 (2002).
24. T. M. Jessell, Neuronal specification in the spinal cord: Inductive signals and transcriptional codes. *Nat. Rev. Genet.* **1**, 20–29 (2000).
25. M. Cohen, J. Briscoe, R. Blassberg, Morphogen interpretation: The transcriptional logic of neural tube patterning. *Curr. Opin. Genet. Dev.* **23**, 423–428 (2013).
26. D. M. Thal, R. Y. Yeow, C. Schoenau, J. Huber, J. J. G. Tesmer, Molecular mechanism of selectivity among G protein-coupled receptor kinase 2 inhibitors. *Mol. Pharmacol.* **80**, 294–303 (2011).
27. J. D. Lowe, H. S. Sanderson, A. E. Cooke, M. Ostovar, E. Tsianova, S. L. Withey, C. Chavkin, S. H. Mubands, E. Kelly, G. Henderson, C. P. Bailey, Role of G protein-coupled receptor kinases 2 and 3 in μ -opioid receptor desensitization and internalization. *Mol. Pharmacol.* **88**, 347–356 (2015).
28. J. Svärd, K. H. Henricson, M. Persson-Lek, B. Rozell, M. Lauth, Å. Bergström, J. Ericson, R. Toftgård, S. Teglund, Genetic elimination of Suppressor of fused reveals an essential repressor function in the mammalian hedgehog signaling pathway. *Dev. Cell* **10**, 187–197 (2006).
29. M. G. H. Gephart, Y. S. Su, S. Bandara, F.-C. Tsai, J. Hong, N. Conley, H. Rayburn, L. Milenkovic, T. Meyer, M. P. Scott, Neuropilin-2 contributes to tumorigenicity in a mouse model of Hedgehog pathway medulloblastoma. *J. Neurooncol.* **115**, 161–168 (2013).
30. G. J. P. Dijkgraaf, B. Aliche, L. Weinmann, T. Januario, K. West, Z. Modrusan, D. Burdick, R. Goldsmith, K. Robarge, D. Sutherland, S. J. Scales, S. E. Gould, R. L. Yauch, F. J. de Sauvage, Small molecule inhibition of GDC-0449 refractory smoothed mutants and downstream mechanisms of drug resistance. *Cancer Res.* **71**, 435–444 (2011).
31. R. L. Yauch, G. J. P. Dijkgraaf, B. Aliche, T. Januario, C. P. Ahn, T. Holcomb, K. Pujara, J. Stinson, C. A. Callahan, T. Tang, J. F. Bazan, Z. Kan, S. Seshagiri, C. L. Hann, S. E. Gould, J. A. Low, C. M. Rudin, F. J. de Sauvage, *Smoothed* mutation confers resistance to a hedgehog pathway inhibitor in medulloblastoma. *Science* **326**, 572–574 (2009).
32. C. S. Pao, B. L. Barker, J. L. Benovic, Role of the amino terminus of G protein-coupled receptor kinase 2 in receptor phosphorylation. *Biochemistry* **48**, 7325–7333 (2009).
33. E. V. Gurevich, J. J. G. Tesmer, A. Mushegian, V. V. Gurevich, G protein-coupled receptor kinases: More than just kinases and not only for GPCRs. *Pharmacol. Ther.* **133**, 40–69 (2012).
34. R. Sterne-Marr, J. J. G. Tesmer, P. W. Day, R. P. Stracquatano, J.-A. E. Cilente, K. E. O'Connor, A. N. Pronin, J. L. Benovic, P. B. Wedegaertner, G protein-coupled receptor kinase 2/G $\alpha_{q/11}$ interaction. A novel surface on a regulator of G protein signaling homology domain for binding G α subunits. *J. Biol. Chem.* **278**, 6050–6058 (2003).
35. A. Beautrait, K. R. Michalski, T. S. Lopez, K. M. Mannix, D. J. McDonald, A. R. Cutter, C. B. Medina, A. M. Hebert, C. J. Francis, M. Bouvier, J. J. G. Tesmer, R. Sterne-Marr, Mapping the putative G protein-coupled receptor (GPCR) docking site on GPCR kinase 2: Insights from intact cell phosphorylation and recruitment assays. *J. Biol. Chem.* **289**, 25262–25275 (2014).
36. V. Ribes, J. Briscoe, Establishing and Interpreting graded Sonic Hedgehog signaling during vertebrate neural tube patterning: The role of negative feedback. *Cold Spring Harb. Perspect. Biol.* **1**, a002014 (2009).
37. T. Oosterveen, S. Kurdija, Z. Alekseenko, C. W. Uhde, M. Bergsland, M. Sandberg, E. Andersson, J. M. Dias, J. Muhr, J. Ericson, Mechanistic differences in the transcriptional interpretation of local and long-range Shh morphogen signaling. *Dev. Cell* **23**, 1006–1019 (2012).
38. J. P. Junker, K. A. Peterson, Y. Nishi, J. Mao, A. P. McMahon, A. van Oudenaarden, A predictive model of bifunctional transcription factor signaling during embryonic tissue patterning. *Dev. Cell* **31**, 448–460 (2014).
39. B. S. Moore, A. N. Stepanchick, P. H. Tewson, C. M. Hartle, J. Zhang, A. M. Quinn, T. E. Hughes, T. Mirshahi, Cilia have high cAMP levels that are inhibited by Sonic Hedgehog-regulated calcium dynamics. *Proc. Natl. Acad. Sci. U.S.A.* **113**, 13069–13074 (2016).
40. L. Vuolo, A. Herrera, B. Torroba, A. Menendez, S. Pons, Ciliary adenylyl cyclases control the Hedgehog pathway. *J. Cell Sci.* **128**, 2928–2937 (2015).
41. D. L. DeCamp, T. M. Thompson, F. J. de Sauvage, M. R. Lerner, Smoothed activates G α_q -mediated signaling in frog melanophores. *J. Biol. Chem.* **275**, 26322–26327 (2000).
42. N. A. Riobo, B. Saucy, C. DiLizio, D. R. Manning, Activation of heterotrimeric G proteins by Smoothed. *Proc. Natl. Acad. Sci. U.S.A.* **103**, 12607–12612 (2006).
43. S. K. Ogden, D. L. Fei, N. S. Schilling, Y. F. Ahmed, J. Hwa, D. J. Robbins, G protein G α_q functions immediately downstream of Smoothed in Hedgehog signalling. *Nature* **456**, 967–970 (2008).
44. M. Barzi, D. Kostrz, A. Menendez, S. Pons, Sonic Hedgehog-induced proliferation requires specific G α inhibitory proteins. *J. Biol. Chem.* **286**, 8067–8074 (2011).
45. F. Shen, L. Cheng, A. E. Douglas, N. A. Riobo, D. R. Manning, Smoothed is a fully competent activator of the heterotrimeric G protein G α_q . *Mol. Pharmacol.* **83**, 691–697 (2013).
46. H. J. Sharpe, G. Pau, G. J. Dijkgraaf, N. Basset-Seguin, Z. Modrusan, T. Januario, V. Tsui, A. B. Durham, A. A. Dlugosz, P. M. Haverty, R. Bourgon, J. Y. Tang, K. Y. Sarin, L. Dirix, D. C. Fisher, C. M. Rudin, H. Sofen, M. R. Migden, R. L. Yauch, F. J. de Sauvage, Genomic analysis of Smoothed inhibitor resistance in basal cell carcinoma. *Cancer Cell* **27**, 327–341 (2015).
47. S. X. Atwood, K. Y. Sarin, R. J. Whitson, J. R. Li, G. Kim, M. Rezaee, M. S. Ally, J. Kim, C. Yao, A. L. S. Chang, A. E. Oro, J. Y. Tang, Smoothed variants explain the majority of drug resistance in basal cell carcinoma. *Cancer Cell* **27**, 342–353 (2015).
48. J. Kim, B. T. Aftab, J. Y. Tang, D. Kim, A. H. Lee, M. Rezaee, J. Kim, B. Chen, E. M. King, A. Borodovsky, G. J. Riggins, E. H. Epstein Jr., P. A. Beachy, C. M. Rudin, Itraconazole and arsenic trioxide inhibit hedgehog pathway activation and tumor growth associated with acquired resistance to smoothed antagonists. *Cancer Cell* **23**, 23–34 (2013).
49. E. F. X. Byrne, R. Sircar, P. S. Miller, G. Hedger, G. Luchetti, S. Nachtergaele, M. D. Tully, L. Mydock-McGrane, D. F. Covey, R. P. Rambo, M. S. P. Sansom, S. Newstead, R. Rohatgi, C. Siebold, Structural basis of Smoothed regulation by its extracellular domains. *Nature* **535**, 517–522 (2016).
50. G. V. Pusapati, C. E. Hughes, K. V. Dorn, D. Zhang, P. Sugianto, L. Aravind, R. Rohatgi, EFCAB7 and IQCE regulate hedgehog signaling by tethering the EVC-EVC2 complex to the base of primary cilia. *Dev. Cell* **28**, 483–496 (2014).
51. S. K. Bronson, E. G. Plaehn, K. D. Kluckman, J. R. Hagaman, N. Maeda, O. Smithies, Single-copy transgenic mice with chosen-site integration. *Proc. Natl. Acad. Sci. U.S.A.* **93**, 9067–9072 (1996).
52. M. Gouti, A. Tsakiridis, F. J. Wymeers, Y. Huang, J. Kleinjung, V. Wilson, J. Briscoe, In vitro generation of neuromesodermal progenitors reveals distinct roles for Wnt signalling in the specification of spinal cord and paraxial mesoderm identity. *PLOS Biol.* **12**, e1001937 (2014).
53. J.-Z. Yu, M. M. Rasenick, Real-time visualization of a fluorescent G α_q : Dissociation of the activated G protein from plasma membrane. *Mol. Pharmacol.* **61**, 352–359 (2002).
54. G. Luchetti, R. Sircar, J. H. Kong, S. Nachtergaele, A. Sagner, E. F. X. Byrne, D. F. Covey, C. Siebold, R. Rohatgi, D. Pan, Cholesterol activates the G-protein coupled receptor Smoothed to promote Hedgehog signaling. *eLife* **5**, e20304 (2016).
55. R. Rohatgi, L. Milenkovic, M. P. Scott, Patched 1 regulates hedgehog signaling at the primary cilium. *Science* **317**, 372–376 (2007).
56. B. G. Novitsch, H. Wichterle, T. M. Jessell, S. Sockanathan, A requirement for retinoic acid-mediated transcriptional activation in ventral neural patterning and motor neuron specification. *Neuron* **40**, 81–95 (2003).
57. F. A. Ran, P. D. Hsu, J. Wright, V. Agarwal, D. A. Scott, F. Zhang, Genome engineering using the CRISPR-Cas9 system. *Nat. Protoc.* **8**, 2281–2308 (2013).
58. S. A. Stewart, D. M. Dykxhoorn, D. Palliser, H. Mizuno, E. Y. Yu, D. S. An, D. M. Sabatini, I. S. Y. Chen, W. C. Hahn, P. A. Sharp, R. A. Weinberg, C. D. Novina, Lentivirus-delivered stable gene silencing by RNAi in primary cells. *RNA* **9**, 493–501 (2003).
59. K. T. Homan, J. J. Tesmer, Structural insights into G protein-coupled receptor kinase function. *Curr. Opin. Cell Biol.* **27**, 25–31 (2014).

Acknowledgments: We are grateful to S. Mohan (Department of Neurology, UC San Francisco) for help with the generation of *Gnas*^{-/-} NIH/3T3 cell lines. We thank A. Lebensohn, B. Schmidt, and R. Dubey for comments on the manuscript. We thank A. McMillan, PhD (Department of Biomedical Data Science, Stanford University School of Medicine) for expert advice on statistical analysis. **Funding:** G.V.P. was supported by a postdoctoral fellowship from the American Heart Association; J.H.K. by the Stanford School of Medicine Dean's postdoctoral fellowship and Jump Start Award for Excellence in Research; M.G. by the Max Delbrück Center for Molecular Medicine in the Helmholtz Association; A.S. by the HFSP LTF (Human Frontier Science Program Long-Term Fellowship) (LT000401/2014-L) and the People Programme (Marie Curie Actions) of the European Union's Seventh Framework Programme FP7-2013 under REA (Research Executive Agency) grant agreement no. 624973. Work in the laboratory of R.R. was supported by NIH grants GM105448, GM112988, and GM118082 to R.R. Work in the laboratory of J.B. was supported by the BBSRC (Biotechnology and Biological Sciences Research Council) (grant reference BB/J015539/1) and the Francis Crick Institute, which received its funding from the Cancer Research UK (FC001051), the UK Medical Research Council (FC001051), and the Wellcome Trust (FC001051; WT098326MA). Work in the laboratory of P.W.I. was supported by the Toh Kian Chui

foundation. **Author contributions:** Conceptualization: G.V.P., J.H.K., J.B., P.W.I., and R.R.; methodology: G.V.P., J.H.K., B.B.P., A.S., J.B., and R.R.; validation: G.V.P. and J.H.K.; formal analysis: G.V.P.; investigation: G.V.P. and J.H.K.; resources: B.B.P., A.S., M.G., R.S., G.L., and P.W.I.; writing (original draft): G.V.P., J.H.K., and R.R.; writing (review and editing): G.V.P., J.H.K., P.W.I., A.S., M.G., J.B., and R.R.; visualization: G.V.P. and J.H.K.; supervision: J.B. and R.R.; project administration: G.V.P.; funding acquisition: J.B. and R.R. **Competing interests:** P.W.I. owns a small amount of stock shares in Curis Inc., a biotechnology company with interests in pharmacologically targeting Hh signaling. All the other authors declare that they have no competing interests.

Submitted 4 August 2017
Accepted 4 December 2017
Published 6 February 2018
10.1126/scisignal.aao5749

Citation: G. V. Pusapati, J. H. Kong, B. B. Patel, M. Gouti, A. Sagner, R. Sircar, G. Luchetti, P. W. Ingham, J. Briscoe, R. Rohatgi, G protein-coupled receptors control the sensitivity of cells to the morphogen Sonic Hedgehog. *Sci. Signal.* **11**, eaa05749 (2018).

G protein–coupled receptors control the sensitivity of cells to the morphogen Sonic Hedgehog

Ganesh V. Puspapati, Jennifer H. Kong, Bhaven B. Patel, Mina Gouti, Andreas Sagner, Ria Sircar, Giovanni Luchetti, Philip W. Ingham, James Briscoe and Rajat Rohatgi

Sci. Signal. **11** (516), eaao5749.
DOI: 10.1126/scisignal.aao5749

GPCRs reduce sensitivity to Sonic Hedgehog

In the developing spinal cord, Sonic Hedgehog (SHH) released from the notochord and floor plate induces overlying neural progenitor cells (NPCs) to differentiate into different neural cell types in a concentration-dependent manner. Puspapati *et al.* found that loss of the G protein–coupled receptor (GPCR) GPR161 sensitized both cultured fibroblasts and NPCs to SHH. The ability of G α_s , which is activated by GPR161, to negatively regulate SHH signaling did not strictly depend on GPR161, suggesting that other GPCRs that couple to G α_s may also attenuate SHH signaling. Although GPCR kinase 2 (GRK2) is proposed to promote SHH signaling by removing GPR161 from the primary cilium, the authors found that GRK2 enhanced SHH signaling independently of GPR161. GRK2, GPR161, and G α_s tuned cellular sensitivity to SHH likely by affecting the extent of protein kinase A activity, a negative regulator of SHH signaling (see also Focus by Sharpe and de Sauvage).

ARTICLE TOOLS

<http://stke.sciencemag.org/content/11/516/eaao5749>

SUPPLEMENTARY MATERIALS

<http://stke.sciencemag.org/content/suppl/2018/02/02/11.516.eaao5749.DC1>

RELATED CONTENT

<http://stke.sciencemag.org/content/sigtrans/11/516/eaar6377.full>
<http://stke.sciencemag.org/content/sigtrans/8/379/ra55.full>
<http://stke.sciencemag.org/content/sigtrans/8/394/ra92.full>
<http://stke.sciencemag.org/content/sigtrans/8/394/fs16.full>
<http://stke.sciencemag.org/content/sigtrans/10/502/eaam7464.full>
<http://stke.sciencemag.org/content/sigtrans/11/516/eaan8660.full>
<http://science.sciencemag.org/content/sci/351/6275/849.full>
<http://stm.sciencemag.org/content/scitransmed/7/291/291ra96.full>

REFERENCES

This article cites 59 articles, 27 of which you can access for free
<http://stke.sciencemag.org/content/11/516/eaao5749#BIBL>

PERMISSIONS

<http://www.sciencemag.org/help/reprints-and-permissions>

Use of this article is subject to the [Terms of Service](#)